

## 3.4 KrF DRIVER

### 3.4.1 KrF Driver System Requirements

The KrF driver system is required to deliver 3.4 MJ, divided equally among 60 beam directions, uniformly distributed over  $4\pi$  steradians, at repetition rate of 6.7 Hz. The energy spatial distribution must be identical for each of the 60 directions and match a given profile; the target diameter is  $d(\text{mm}) = 5.6 (E(\text{MJ})/4)^{1/3} = 5.3 \text{ mm}$ .<sup>3.46</sup> Power uniformity among the 60 beams should be  $\leq 5\%$  rms. Random beam mispointing of  $\sim 10\%$  rms of the target radius can be tolerated. The temporal distribution of energy in the pulse will be defined for an operating system, but is not defined for this study. Nominal peak power is defined as  $P(\text{TW}) = 240 E(\text{MJ})^{2/3} = 5.4 \times 10^{14}$  watts; an approximate pulse duration is thus  $E/P = 6.3 \text{ ns}$ .

We have assumed the NRL, NIKE system approach for direct drive targets of "echelon-free ISI" in which a desired intensity profile is imaged onto the target through the laser chain, using partially coherent light. Broadband KrF emission with  $\Delta\nu/\nu \sim 0.1\%$  is used to provide coherence times  $< 1 \text{ ps}$  and thus allow rapid spatial averaging on the target. It is an approach which utilizes imaging of a front end aperture through the whole amplifier chain, including angular multiplexing, to the target. It thus allows for the target beam spatial profile to change during the pulse and thereby take advantage of the higher direct drive target gains that occur for a system that can zoom the target illumination spot as the target diameter decreases during irradiation. We have not taken credit for zooming in the base case parameters cited earlier (i.e.,  $G = 118$  at  $E = 3.4 \text{ MJ}$ ).

### 3.4.2 Background

There are several goals in the design of a KrF driver system for IFE: 1) high operating efficiency, 2) low capital cost, 3) technical credibility, 4) high availability/reliability, and 5) low operating costs. In this study we were to assume technology that could be mature in the year 2040, and a plant that would be the tenth of its kind. We have assumed physics issues as they are understood today, such as laser efficiency based on our best models for kinetics and extraction as anchored by available data; we have not, for example, assumed the finding of some "new" laser gas mixture by the year 2040 that would increase the laser efficiency by another 10%.

In creating a design, we have focused on how to optimize overall laser system operating efficiency because of the continuous operation of the plant. In a single pulse test facility, capital cost is the more dominant consideration, and efficiency is mainly considered in the context of its effect on capital cost.

### 3.4.2.1 Direct vs. Indirect Drive

The gain curves provided for this study by DOE clearly favored direct drive. We saw no difficulty with making a laser system for this choice and no advantage for the laser system for choosing indirect drive. As far as the laser driver system is concerned, we believe we could meet the requirements for an indirect drive target with a very similar system at similar cost. The ability of KrF driver systems to meet the brightness requirements for indirect as well as direct drive targets was described in a paper in Osaka in 1991.<sup>3,47</sup> In the Osaka paper it was concluded that for an indirect drive spot diameter of 1.5 mm, 3 MJ on target with 50 m to the final focusing optics, that a beam quality of 5.2 times the diffraction limit was adequate. It was then shown that with reasonable assumptions for phase errors introduced through the system that 0.32 waves rms of phase error accumulate, which is consistent with the beam quality requirement. Since direct drive targets have larger gain, and there is little practical difference in geometry of beam delivery to the target, it seems sensible to select the direct drive option. Should this story change at a future date and indirect drive be the favored target choice, an appropriate KrF driver system design could be generated.

### 3.4.2.2 E-Beam Pumping

KrF laser kinetics and extraction physics have been studied in some detail since the first KrF lasing was achieved in 1975. Despite promising theoretical predictions for discharge and e-beam + discharge pumping, these approaches have not come close to the intrinsic efficiencies achieved by pure e-beam pumping (intrinsic efficiency is (laser output energy)/(energy deposited in the laser gas mixture);  $\eta_I \sim 14.5\%$  for our present design parameters). Low efficiency of the e-beam itself has been an area of concern for e-beam pumped systems; however, we have recently published a description of a technology for e-beams that will allow them to operate at high average power, for long durations, and at high efficiencies - constrained only by the albedo of the laser gas mixture and the foil.<sup>3,48</sup> E-beam efficiencies of  $\eta_{eb} > 80\%$  are possible in the system we describe herein with 1 atm of 50% Ar + 50% Kr (+small amount of F<sub>2</sub>) mixtures and titanium foils;  $\eta_{eb}$  approaching 90% should be possible with beryllium/aluminum foils. In these designs the e-beam is not allowed to intercept the foil support structure (i.e., the so called "hibachi" structure). The ability to achieve such "non-intercepting" operation has been experimentally demonstrated at Textron. This technology, coupled with the high voltage, cable based pulse forming lines (Section 3.4.4.1), a double foil system for removal of steady state waste heat (Section 3.4.4.2), and the demonstrated high intrinsic efficiencies (14.5%) at high pump rate (400 kW/cm<sup>3</sup>) and high specific energy (30 J/l-atm for our design projections) for e-beam pumping make this approach our clear choice.

### 3.4.2.3 Angular Multiplexing

Pulse shortening from the many hundreds of nanoseconds, at which large e-beam pumped amplifiers may be efficiently made, to the ~ 6 ns required for target irradiation may be reliably and efficiently achieved, at reasonable system cost, by the use of angular multiplexing. This pulse compression approach has been developed for the Aurora (Los Alamos) and Nike (Naval Research Lab.) systems, as well as others at Rutherford in England, at the University of Alberta in Canada, and the Electrotechnical Laboratory in Japan. In some of these systems, angular multiplexing was used in concert with Raman beam combining. We have not utilized Raman technology because we believe we can achieve adequate beam quality from our amplifiers without the added cost and complication of Raman conversion.

### 3.4.2.4 Generic Driver System Description

The KrF driver system consists of 1) a front-end which produces a pulse of the desired bandwidth and temporal and spatial intensity characteristics, 2) several stages of intermediate amplification and progressive temporal/angular multiplexing, 3) final amplification by large e-beam pumped 2-pass amplifiers, and 4) demultiplexing and beam delivery to the reactor building. This is illustrated in Fig. 3.66. (Note that here and throughout this chapter, we describe the design of a 3.6 MJ driver, which is slightly larger than the eventually selected reference design point of 3.4 MJ.) In the reactor building, the beams are brought through a mirror system that provides neutron protection to the laser stages and brings equal amounts of KrF illumination to the target from 60 uniformly spaced directions by way of grazing incidence metal mirrors, which are the only optical element subjected to direct neutron flux. The Ultimate Amplifiers (UA's) in our system operate with a two-pass gain of 16, so the Penultimate Amplifiers (PA's) only supply ~ 6% as much energy. From this, it is clear that the efficiency and the capital cost of the laser driver system is dominated by the UA's. Because of this our design discussion at the conceptual stage focuses on consideration of these amplifiers, how their efficiency may be optimized, and how they may most effectively be assembled into an architecture that satisfies the target requirements. Our approach for efficiency optimization is described in Section 3.4.3.

### 3.4.2.5 Laser Reject Heat Utilization

With a KrF laser intrinsic efficiency of ~15%, it is clear that a large fraction of the input energy ends up as waste heat. In 1987 Pendergrass<sup>3,49</sup> showed that the effective laser efficiency could be greatly enhanced by thermodynamically making use of the waste heat. For example, a driver system with 10% wall plug efficiency, for which 70% of the waste heat could be recovered at 250°C or higher and converted with 75% of Carnot efficiency into electricity ( $75\% \cdot 45\% = 34\%$ ) would result in an effective laser efficiency of 12.7% - an improvement of 27%. The waste

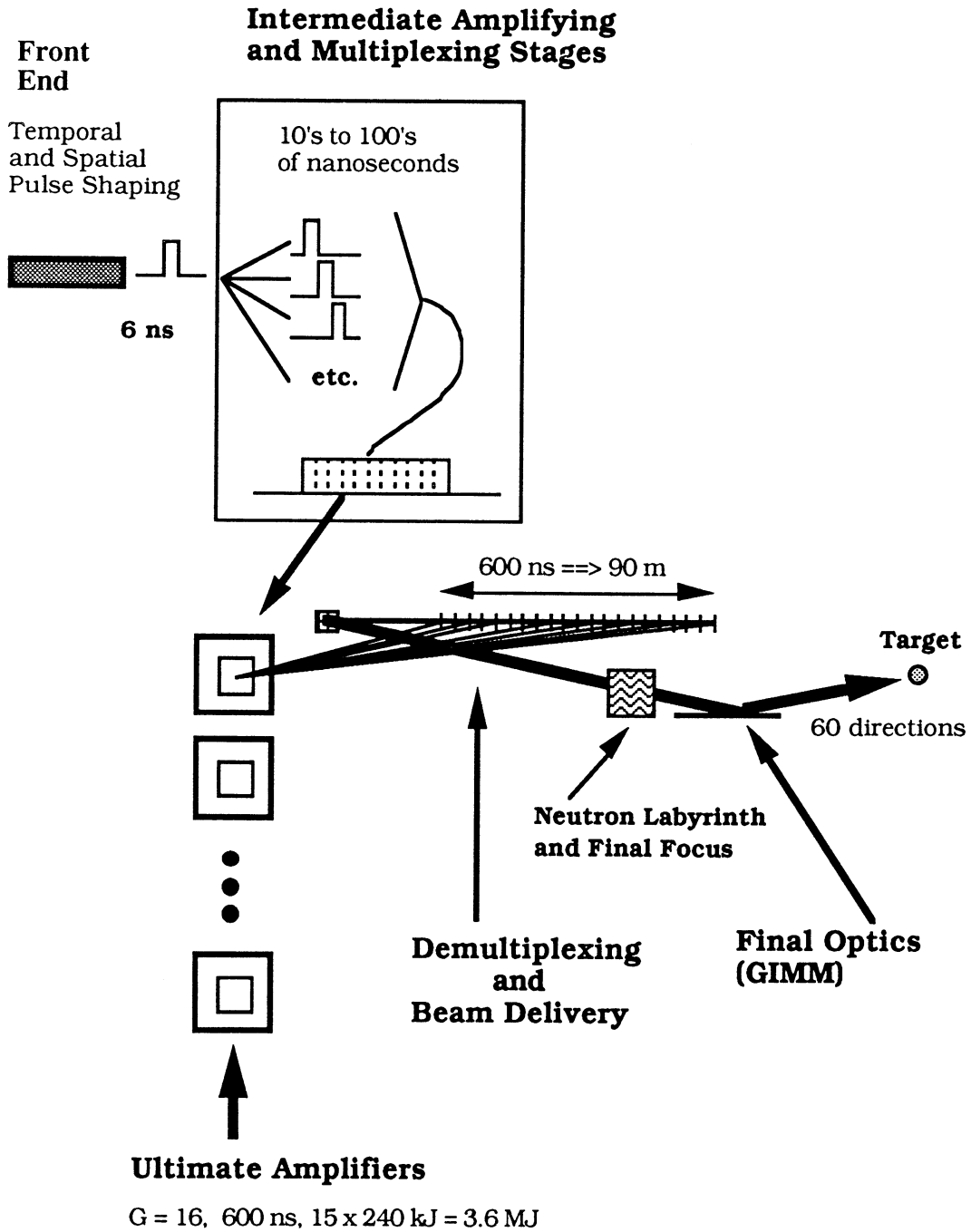


Fig. 3.66. Generic diagram of KrF laser driver system.

heat recovery assumptions are reasonable, because most of the waste heat ends up in the laser gas mixture, which is being circulated in a flow loop with heat exchangers that are already required to remove the waste heat for purposes of recycling the gas. The  $\Delta T$  due to  $\sim 300$  J/liter of energy deposition is  $\sim 320^\circ\text{C}$  after pressure equilibration and is diminished, on average, by a factor of 1.3 due to the "flush factor" of 1.3 of the flow system design. This design has some unpumped gas passing through the laser cavity following each slug of e-beam pumped gas that is flushed out after each laser pulse. Thus we may assume  $50^\circ\text{C}$  gas temperature going into the laser cavity,  $\Delta T = 320^\circ$  diluted to  $\Delta T \sim 250^\circ$ , giving an average temperature of  $T = 300^\circ\text{C}$  going to the heat exchanger.

### 3.4.3 Amplifier Efficiency Optimization

High overall efficiency of the final or ultimate amplifiers (UA's) as used in the system is key for determining the overall driver system efficiency. To determine the best values for the design parameters, we first write the overall amplifier efficiency as the product of its identifiable components, which are illustrated in Fig. 3.67.

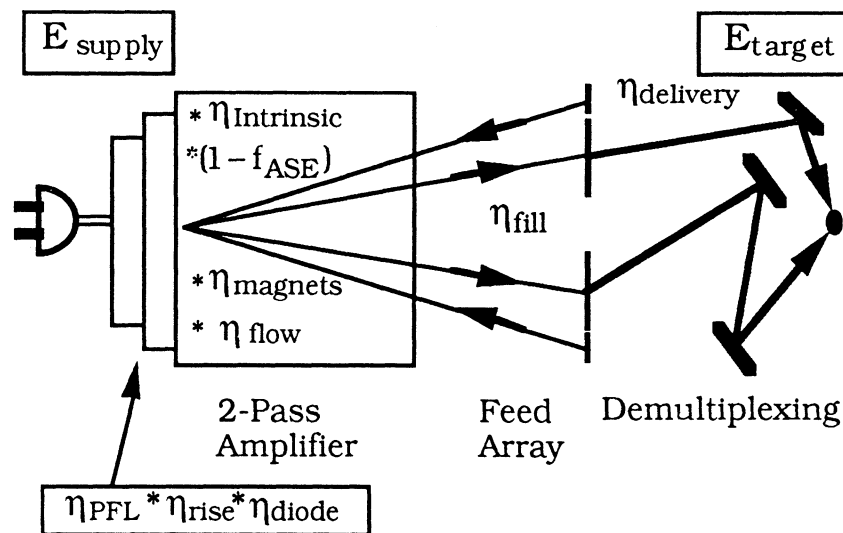


Fig. 3.67. Schematic of KrF amplifier showing the efficiency components contributing to the overall amplifier efficiency.

Thus we write:

$$\eta_{\text{LaserSystem}} = \eta_{\text{PFL}} \cdot \eta_{\text{RiseTime}} \cdot \eta_{\text{Diode}} \cdot \eta_{\text{Intrinsic}} \cdot \eta_{\text{ASE}} \cdot \eta_{\text{Magnets}} \cdot \eta_{\text{Flow}} \cdot \eta_{\text{Fill}} \cdot \eta_{\text{Delivery}}$$

where the terms refer respectively to:

$\eta_{\text{LaserSystem}}$  Efficiency of converting electricity, taken from the gross plant output, into photon energy impinging on the target. Known as "wall plug efficiency" in other contexts. We are assuming the flow of power to the ultimate amplifiers and on to the targets dominate this term; it will be reduced a small amount by the different efficiencies of the preceding amplifier stages. We note that the immediately preceding stage, the penultimate amplifier stage, uses identical cavities to the ultimate stage, and thus will run at approximately the same efficiency.

$\eta_{\text{PFL}}$  Efficiency of charging the pulse forming line (cables), ~ 90%.

$\eta_{\text{RiseTime}}$  Losses due to expenditure of energy during the rise and fall time of the e-beam current, when non useful pumping of the medium occurs. This term is dependent on L/Z (inductance/impedance) for the e-beam load, and thus becomes unfavorable for large cathode areas and short pump durations. For very large amplifiers it makes sense to segment the e-beams, each with its own return current path, on each side of the amplifier. This also has the benefit of lowering the magnitude of the e-beam self B-field.  $\eta_{\text{Rise Time}} \sim 1/[1+(\tau_{\text{rise}}/\tau_{\text{extract}})] \sim 94\%$  in our 60 kJ design.

$\eta_{\text{Diode}}$  Efficiency of the diode itself - mainly due to back scatter determined by the foil system and the laser gas mixture. For our 1 atm Ar:Kr ~ 50%:50% mixtures, e-beam voltage of ~610 kV, and beryllium/aluminum foils, the albedo is ~ 91%. For our "non-intercepting" e-beam design, this is the limiting value for  $\eta_{\text{Diode}}$ . We have, however, assumed 90% efficiency exclusive of the albedo effects, so an overall  $\eta_{\text{Diode}} = 82\%$  is used.

$\eta_{\text{Intrinsic}}$  =  $\eta_{\text{Formation}} \cdot \eta_{\text{Extraction}}$ , the formation efficiency of upper laser states (KrF\*) at the given pump rate and laser gas composition and pressure, multiplied by the extraction efficiency for the given length of pumped laser gas, unpumped but absorbing end regions adjacent to the window and mirror, for two-pass extraction, with an input flux (W/cm<sup>2</sup>) consistent with operating at a specified two-pass amplifier gain.  $\eta_{\text{Intrinsic}} \sim 14.5\%$  for our design conditions.

$\eta_{\text{ASE}}$	= $(1-f_{\text{ASE}})$ , where $f_{\text{ASE}}$ is the fractional loss of extractable energy due amplified spontaneous emission; we have used an analytical correlation formula developed at Los Alamos. <sup>3.50</sup> It is dependent on the Sullivan parameter $Su = GR_swh/L^2$ , where $G$ is the amplifier two-pass gain, $R_s$ is the sidewall reflectivity at the laser wavelength, $w$ is the width, $h$ is the height, and $L$ is the length. $\eta_{\text{ASE}} \sim 85\%$ at our design conditions.
$\eta_{\text{Magnets}}$	This term accounts for the power which must be expended to operate the magnets. It is $\sim 99\%$ or higher since we only require $\sim 6$ kG fields and we use superconducting magnets.
$\eta_{\text{Flow}}$	This term accounts for the power which must be expended to operate the flow loop.
$\eta_{\text{Fill}}$	The fill factor refers to the degree with which one fills the amplifier volume with two-way photon flux, for efficient extraction, given that we need to angularly encode about 100, time multiplexed, beams per amplifier. This factor depends on the size of the mirrors we need to use, which depends on the average fluence ( $\text{J}/\text{cm}^2$ ) we design for on the input/output "feed" array of mirrors and the separation distance from the amplifier to the feed array. Finally, there is a constraint in how close output beam angles may be due to small angle scattering by the output window and the need to keep light from one angularly encoded channel from entering another channel and giving a pre-pulse of energy on the target. We use $\alpha \geq 4$ mrad. <sup>3.51</sup> $\eta_{\text{Fill}} \sim 97\%$ for a nominal 60 kJ size amplifier with $5 \text{ J}/\text{cm}^2$ optics and $\alpha = 4$ mrad. The separation distance required is $\geq 24$ m in this case.
$\eta_{\text{Delivery}}$	Small reflection losses ( $\sim 0.5\%$ per surface) on each of the mirrors in route to the target ( $\sim 8$ surfaces) give $\sim 96\%$ for this term. Beam delivery is done in vacuum so there are no losses due to absorbing or scattering gasses.

Using our KrF kinetics code and amplifier extraction code, we generated parametric expressions for  $\eta_{\text{Intrinsic}}$  as a function of gas composition, amplifier gain  $G$ , amplifier length  $L$ , pump rate  $P$ , and extraction time  $\tau_e$ . We assumed enough  $F_2$  for the amount of total pumping  $\text{J}/\text{liter} = P\tau_e$ , given our experience with data and calculations fitting data to this parameter. We also did calculations using a Los Alamos set of rate constants in our code and found no important difference in the calculated results for net amplifier efficiency.

With all of the component efficiencies expressed analytically, we performed parametric variations and created the following graphs of the results. In the following examples we used the

following parameters: Two-pass  $G = 12$ ,  $E = 240$  kJ at the output window, 1 atm Kr + F<sub>2</sub> at 323 K, 400 kW/cm<sup>3</sup> pumping, 600 ns extraction, and  $h/w = 2$ . We then varied the length, which occurs at almost constant volume, because the output energy was specified and the efficiency varies slowly over most of the range of interest. Thus, the output window area goes down as  $\sim 1/\text{length}$ , but at constant  $h/w$ .

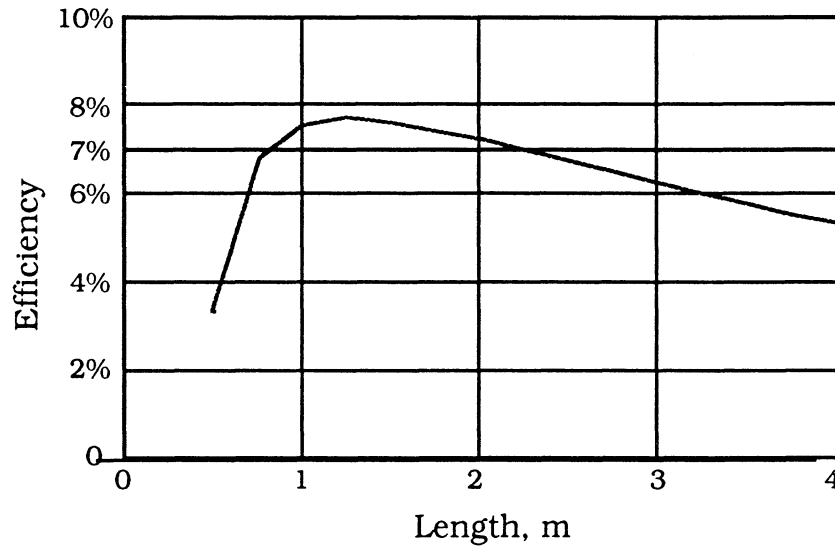


**Fig. 3.68.**  $\eta_{\text{LaserSystem}}$  vs pumped gas length; Two-pass  $G = 12$ ,  $E = 240$  kJ at the output window, 1 atm Kr + F<sub>2</sub> at 323 K, 400 kW/cm<sup>3</sup> pumping, 600 ns extraction, and  $h/w = 2$ .

Figure 3.68 shows a peak efficiency of  $\sim 7.6\%$  at  $\sim 1.25$  m of length. To explain why the efficiency curve has a peak, we next examine the four components which are responsible for the shape of the curve in Fig. 3.68.

Figure 3.69 shows  $\eta_{\text{ASE}}$  and the intrinsic efficiency as a function of amplifier length. At short lengths the amplifier has large transverse dimensions which give rise to large ASE losses; the parameter  $S_u \sim hw/L^2$  is highly sensitive since  $hw \sim 1/L$  for our constant amplifier energy. Intrinsic efficiency drops off at long lengths because of the departures of the average total extracting flux,  $[\phi_{\text{left}} + \phi_{\text{right}}]$ , from optimum extracting flux,  $\phi_{\text{opt}} = [\sqrt{(g_0/\alpha)} - 1]$ , imposed on the solution by the assumed gain and other design parameters.

Figure 3.70 shows  $\eta_{\text{Fill}}$  and  $\eta_{\text{Flow}}$  versus amplifier length. The efficiency term attributable to the flow power requirement becomes low at short amplifier lengths because the flow dimension  $h \sim 1/\sqrt{L}$  (at constant  $h/w$ ), and flow power  $\sim$  Mach number squared  $\sim h^2$ . The Fill Factor monotonically decreases with  $L$  because the aperture is getting smaller at the same time the

length is increasing, both of which increase the fraction of partially extracted regions for a given feed array size and location.

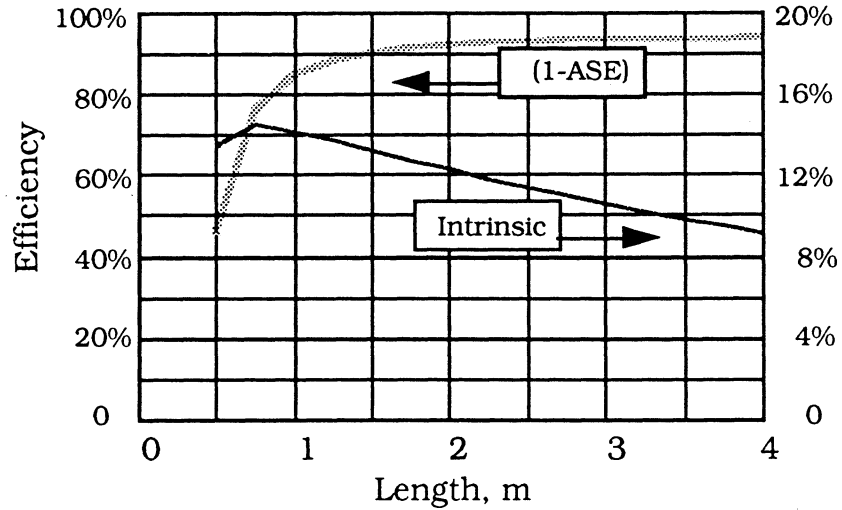


Fig. 3.69.  $\eta_{ASE} = (1-f_{ASE})$  and intrinsic efficiency vs length for the conditions of Fig. 3.68.

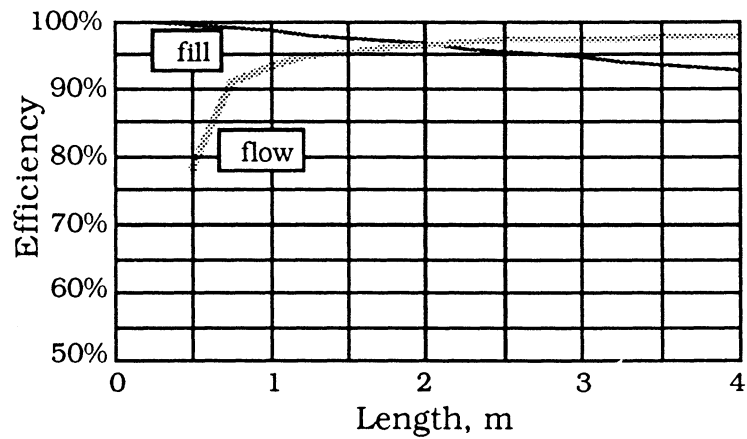
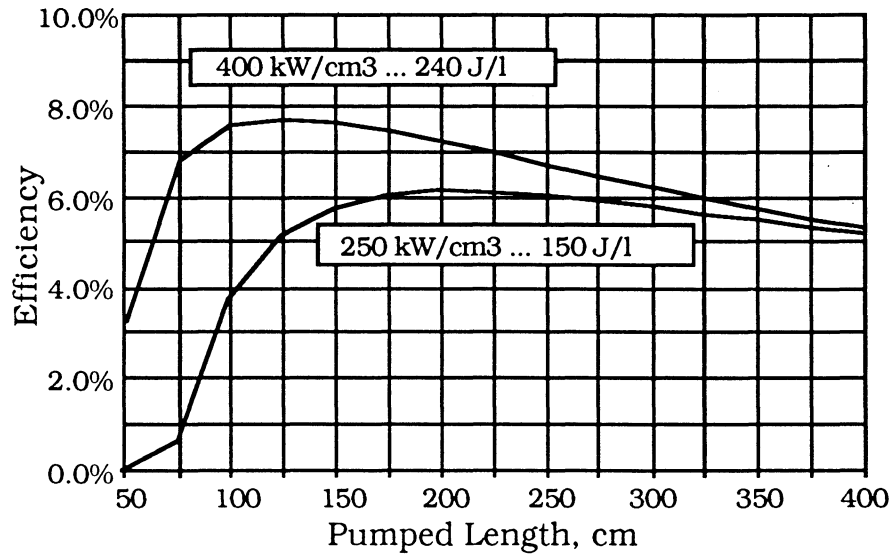


Fig. 3.70. Fill factor and  $\eta_{Flow}$  vs length for the conditions of Fig. 3.68.

Figure 3.71 shows the benefit of our choice of a high pump rate,  $400 \text{ kW/cm}^3$ , relative to a more traditional choice of  $250 \text{ kW/cm}^3$ . The higher pump rate gives higher efficiency, and it gives it at a relatively short design length. Even higher pump rates did not further increase the efficiency significantly.



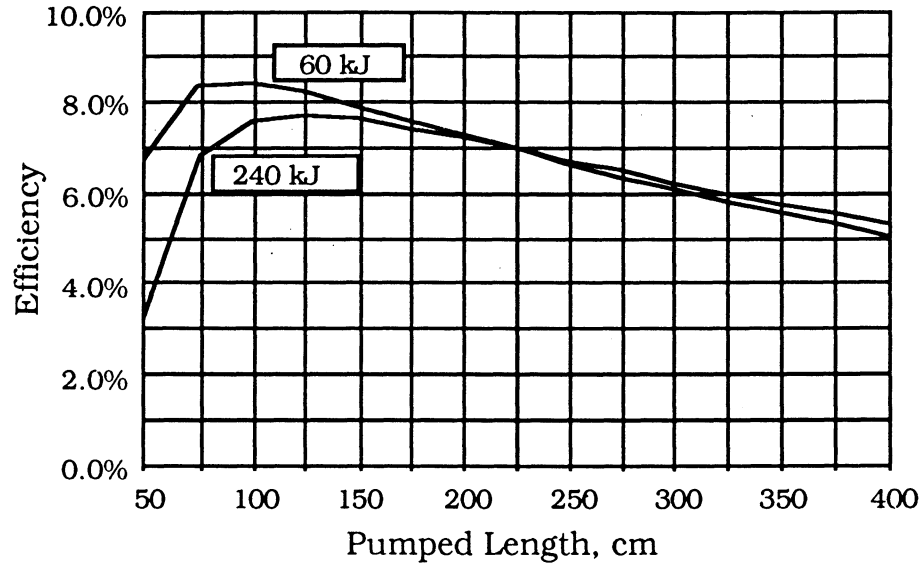
**Fig. 3.71.**  $\eta_{\text{LaserSystem}}$  at pump rates of  $250$  and  $400 \text{ kW/cm}^3$  vs length; energy deposited during  $600 \text{ ns}$  pulse lengths given;  $1 \text{ atm Kr} + \text{F}_2$ , two pass,  $G=12$  amplifier extraction.

Figure 3.72 shows the benefit on efficiency of operating with smaller amplifier size. We also calculated efficiency for even smaller amplifier sizes, with no further improvement of note.

Figure 3.73 shows the beneficial effect of waste heat recovery, as discussed in Section 3.4.2.5 on the de facto laser efficiency when used in a total system which may efficiently make use of the waste heat. In the systems analysis, the efficiency is accounted for in the thermal conversion efficiency of the power cycle.

We have also examined the effect of amplifier two pass gain  $G$  in the vicinity of our interest,  $G = 10$  to  $20$ . The net effect is small; the higher gains had better intrinsic efficiency but offsetting ASE losses.

The choice of gas mixture is one of choosing the relative fractions of argon and krypton since  $\text{F}_2$  is determined by the Joules/liter desired. Our code calculations show best intrinsic efficiency at  $\sim 50\%$  argon, but there is little change in going to pure krypton. More krypton means higher e-beam voltage, lower current. Lower voltages are an advantage in reducing standoff



**Fig. 3.72.**  $\eta_{\text{LaserSystem}}$  for 60 kJ and 240 kJ amplifiers; 1 atm Kr + F<sub>2</sub>, G=12 two pass amplification, 600 ns extraction, 400 kW/cm<sup>3</sup> pumping.

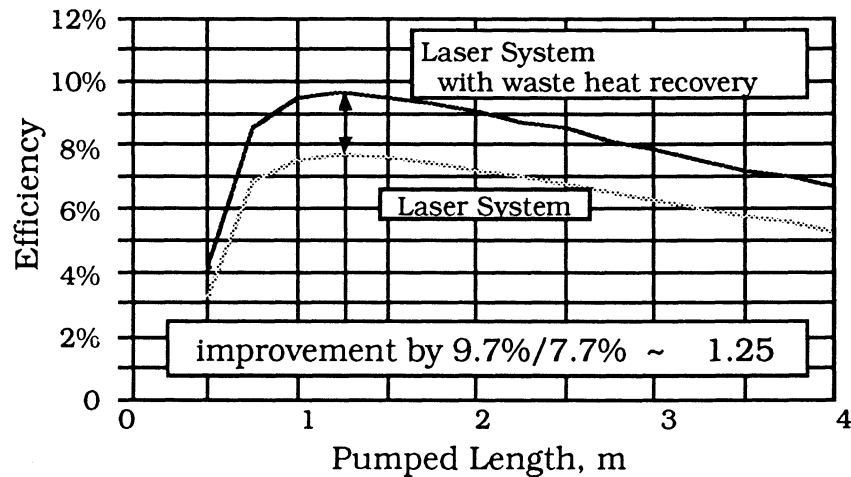


**Fig. 3.73.**  $\eta_{\text{LaserSystem}}$  as shown in Fig. 3.68 and as it is with credit given for utilization of waste heat as discussed in Section 3.4.2.5.

distances, and thus inductance, but lower voltage/higher current means lower impedance; since the ratio  $L/Z$  determines rise time, these are competing effects. We can design a diode for either case, and the cathode technology we invoke has been demonstrated at the  $\mu\text{coulombs/cm}^2$  that we require for 50% argon, so we have made that choice to optimize efficiency.

We have chosen 60 kJ as the nominal amplifier size because it has higher efficiency, has no higher capital cost per Joule of electrical input energy to the laser amplifier, and is more

attractive for development in terms of size of components and operating voltage. The 60 kJ size leads to a very reasonable architecture, as we show later. Larger amplifiers would require longer pulse lengths (to keep  $\tau_{\text{rise}}/\tau_{\text{extract}}$  reasonable), with greater number of multiplexing channels, though probably not more mirrors in number since there are more amplifier cavities in the system. Larger amplifiers would require larger e-beam voltages, and larger B-fields. Segmented e-beams is a way of helping this problem, but since each requires its own return current path, there appears no decisive advantage over more, smaller amplifiers. Amplifiers even smaller than 60 kJ would have no appreciable efficiency advantage and would have lower diffraction limited optical performance because of smaller final optic dimension ( $w$ ) and angular beam spread  $\sim \lambda/w$ , where  $\lambda$  is the KrF wavelength.

Our choices for amplifier specifications are given in Table 3.16. Most of the terms are familiar to the reader by now, but we note "d" is the "dead" space of unpumped laser gas adjacent to amplifier window and mirror. The flush factor is the ratio of  $v\tau/h$ , where  $v$  is the flow velocity in the cavity,  $\tau$  is the pumping time, and  $h$  is the cavity height.  $K$  is the ratio of the total amount of flow losses ( $\Delta p$  pressure drop) in the flow loop per cavity divided by the dynamic pressure in the laser cavity ( $q = 1/2\rho v^2$ ). Fluence is the average fluence on the short pulse (6 ns) optics of the feed array, demultiplexing optics, etc. We assumed two sided e-beam pumping. Some of the amplifier operating parameters given in Table 3.17.

**Table 3.16. Amplifier Cavity Specifications Chosen for KrF Laser Driver Design**

E on target	60 kJ	l (optical)	1 m
Ar in Kr	50%	h (flow)	2 m
Pressure	1 atm	w (e-beam)	1 m
T <sub>initial</sub>	50°C	d, unpumped gas	15 cm
Pumping	400 kW/cm <sup>3</sup>	Flush factor	1.3
$\tau_{\text{extract}}$	600 ns	K ( $\Delta p/q$ )	6
Gain	16	Fluence	5 J/cm <sup>2</sup>
PRF	7 Hz		

**Table 3.17. Amplifier Operating Parameters**

e-beam voltage	610 kV	$\tau_{\text{rise}}/\tau_{\text{extract}}$	6.1%
J <sub>Diode</sub>	40.6 A/cm <sup>2</sup>	$\eta_{\text{Intrinsic}}$	14.5%
Z <sub>Diode</sub>	0.6 ohms	$\eta_{\text{Net}}$	7.6%
L	23 nH	B <sub>Applied</sub>	6 kGauss

### 3.4.4 Final Amplifier Technology

#### 3.4.4.1 Pulse Power

For pulses as short as 0.6 msec, it becomes difficult to design a lumped element PFN with sufficiently low inductance as to give fast rise and fall times. There are two well-established PFL variants which are more suitable, based on water and paper-oil dielectrics, respectively. Water lines have been the choice in virtually all previous studies, most of which are oriented toward single pulse test facilities.<sup>3.52-55</sup> The paper-oil system, available in cable form, has been developed in recent years for high energy, high rep rate DoD applications. Its dielectric constant is high enough that it is competitive on a power per unit area basis. In addition it has a much higher resistivity so that a slow wave form or even DC charging is possible. In contrast, the resistivity of de-ionized water is such that unacceptable losses occur for charging times of more than 2  $\mu\text{sec}$ , unless the water has antifreeze added and is cooled.

The paper-oil system has been tested at Avco/Textron at charge voltages of 800 kV and 50 Hz repetition rate, delivering 15 kJ/pulse in 1.6  $\mu\text{sec}$  flat top wave forms. In this experiment the cable was charged using a pulse (step-up) transformer with a charging time of 30  $\mu\text{sec}$ . A cable and cable termination have been fabricated for 1.5 MV, but have not yet been tested.

Because of leakage inductance, which is inevitable in high voltage pulse transformers, it is not possible to design high energy transformers which will transfer charge to a water line in less than  $\sim 2 \mu\text{sec}$ , so a Marx generator is required. A Marx could also be used to charge cables; however, in the present study we have selected a pulse transformer approach with cables because of better reliability from the fewer number of internal switches, with consequent lower maintenance. Thus, the two systems we focused on for final selection were a Marx + Water Lines system versus a Modulator + Pulse Transformer + Cable PFL system. The two systems are illustrated in Figs. 3.74 and 3.75.

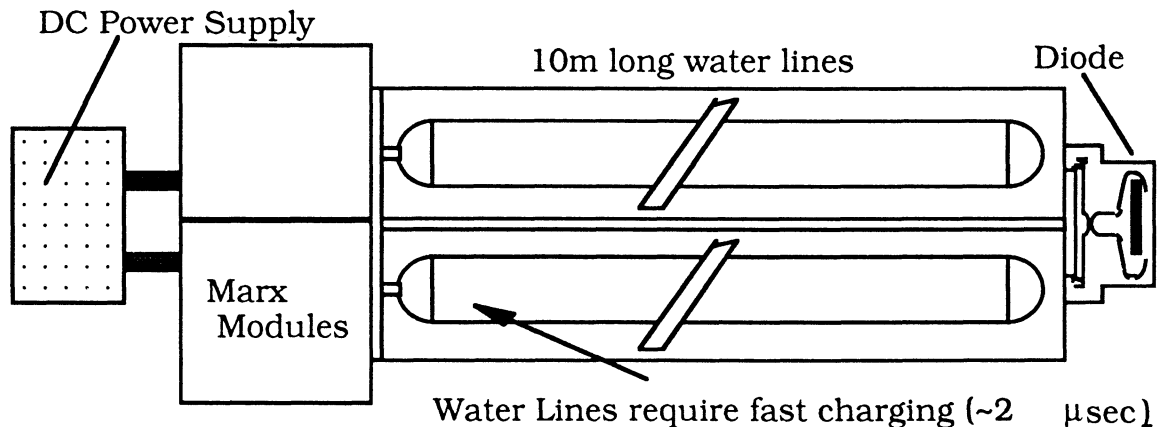
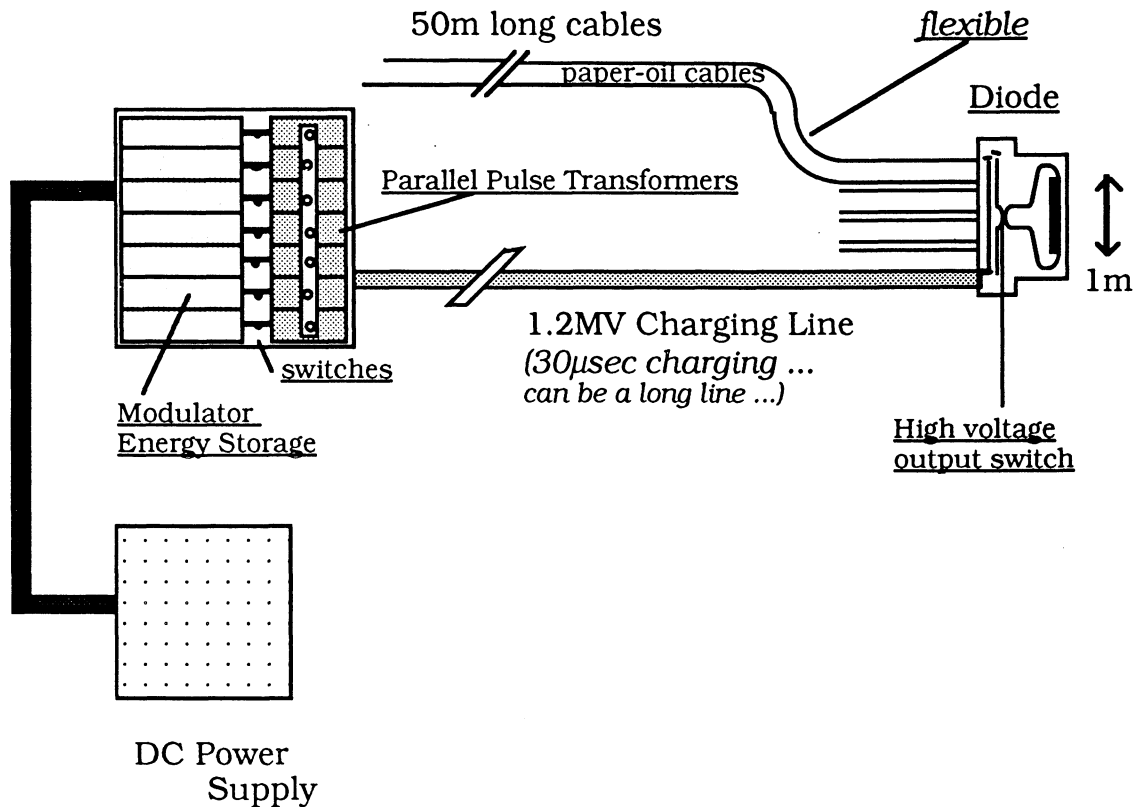


Fig. 3.74. Pulse power system with Marx driven water line PFL.



**Fig. 3.75. Pulse power system with cable PFL and pulse transformer charging.**

A fundamental performance parameter of a PFL is the power per unit cross sectional area that it can supply. We have compared water lines and cables of inner radius "a" and outer radius "b" with dielectric constants of  $K = 81$  and  $3.4$ , respectively. Cooled water has  $K = 45$ . We make use of the following equations:<sup>3.57</sup>

Impedance of a coax cable or water line is

$$Z = 60 \frac{1}{\sqrt{K}} \ln\left(\frac{b}{a}\right) \text{ ohms.}$$

Electric field at the surface of the center conductor is

$$E_a = \frac{V}{a \cdot \ln\left(\frac{b}{a}\right)}$$

Capacitance per unit length is

$$C = \frac{2\pi K \epsilon_0}{\ln\left(\frac{b}{a}\right)}$$

Stored energy per unit length is

$$E = \frac{1}{2} CV^2 = \pi K \epsilon_0 a^2 E_a^2 \ln \left( \frac{b}{a} \right)$$

The line delivers power at voltage  $V/2$  into a matched load impedance  $Z$ ; thus the line power is

$$W_L = \frac{V^2}{4Z} = \frac{a^2 \sqrt{K} E_a^2}{240} \ln \left( \frac{b}{a} \right)$$

If we assume a number of parallel lines are required, each with an outer diameter of  $2R$  and an area of  $4R^2$  in a stacked array, then the power delivered per unit area is

$$W_u = \frac{a^2 \sqrt{K} E_a^2}{960 R^2} \ln \left( \frac{b}{a} \right)$$

Thus in comparing water and paper-oil, the relative figure of merit is  $\sqrt{K} \cdot E_a^2$ . We next consider the allowable electric stress.

The allowable electric stress for 50% probability of breakdown in water is given by Martin<sup>3.57</sup> as

$$F t^{1/3} A^{1/10} = k$$

where  $F$  is in MV/cm,  $t$  is in  $\mu\text{sec}$ , and  $A$  is electrode area in  $\text{cm}^2$ . The parameter  $k$  is  $k^- = 0.6$  at the negative electrode, and  $k^+ = 0.3$  at the positive electrode. In addition to this consideration, one needs to apply a de-rating factor to provide for a lower probability of breakdown. For a  $10^{-4}$  probability, the field stress should be reduced to 60% of  $F$  as given above, based on material from Physics International as reported by Parks.<sup>3.58</sup> For even lower probabilities, as we presumably would desire, the behavior of the curve is suggestive of very little additional de-rating being required, although further work is clearly needed. As an example, the storage of 500 kJ (approximately what is needed for one 60 kJ laser cavity) will require an electrode area of  $A \approx 6 \times 10^5 \text{ cm}^2$ ; we assume the inner electrode, which carries the greatest stress, is at negative polarity, and the charging time is 2  $\mu\text{sec}$ . In this case we get  $E_a = 75 \text{ kV/cm}$ . For a total system with 3.6 MJ laser energy on target, the waterline electrode area is  $\sim 80$  times larger, which implies an  $80^{0.1} = 1.5$  further de-rating to  $E_a \approx 50 \text{ kV/cm}$ .

For paper-oil storage, the DC insulator strength is 1 MV/cm in small volumes ( $\sim 10^4 \text{ cm}^3$ ). If we de-rate by  $(\text{Volume})^{0.1}$ , use  $7 \times 10^6 \text{ cm}^3$  for 500 kJ so the volume de-rating is 50%, and use a factor of 0.7 on the allowable field stress for pulsed operation, then we would obtain  $E_a = 350 \text{ kV/cm}$ . There is presumably further de-rating for the volume associated with the total system, but we note that the de-rating for paper oil with increasing volume is probably not as

severe as it is for a homogeneous insulator such as liquid water because of the way the two components break up the incipient path of breakdown channels. Therefore, we will stay with 350 kV/cm for our total laser system.

Returning to our figure of merit of  $\sqrt{K \cdot E_a^2}$ , for water vs paper oil we have  $\sqrt{81 \cdot 50^2} = 22,500$  and  $\sqrt{3.4 \cdot 350^2} = 226,000$ ; the paper-oil is preferable by a factor of 10 in power per unit area delivery capability. To complete the comparison, we need to recognize the requirement for a field grading structure for the termination, at the diode, of these two different approaches. We estimate the termination of the cables can be done with an outer radius of  $R = 1.6b$ , where "b" is the outer electrode radius of the cable. For water lines, careful present day designs have line center separations of  $1.2b$ . These estimates lead to a reduction in the paper-oil advantage by  $(1.2/1.6)^2 = 56\%$  to 5.6 more power per unit area for cables than for water.

In absolute terms, we now estimate the power per unit area for paper-oil cables, with terminations, at  $1.7 \times 10^7$  W/cm<sup>2</sup>; waterlines would be lower by a factor of 5.6. This may be compared with a diode requirement of  $600 \text{ kV} \cdot 40 \text{ A/cm}^2 = 2.4 \times 10^7$  W/cm<sup>2</sup>. Thus, we need a 40% reduction in area. This can be accomplished with a transition section incorporating the high voltage output rail gap switch, which we will show in the next section. Finally, we note that further improvements in design electric field stress may come with additional work devoted to this goal; cable development to date has been for power transmission applications, for which low stored energy is desired.

Cable pulse forming lines have very low residual resistivity, possibly dominated by resistively graded terminator resistances, so they can be charged on a relatively long time scale of 30 to 50  $\mu$ sec - limited by leakage inductances. Therefore, one may use a pulse transformer rather than a Marx bank for their charging. This technology has been demonstrated at repetition rates up to 100 Hz, delivering 40 kJ at 1.5 MV.<sup>3.59</sup> Energy scaling of this, at constant voltage, is possible through an increase in the cross sectional area of the transformer core; we expect Energy  $\approx$  Area<sup>1.5</sup>. At 1.5 MV it appears possible to scale to at least 100 kJ per transformer. Thus, one could charge multiple cables with one pulse transformer and switch. The primary of the transformer must be fed by a modulator in which the Coulomb transfer is greater than that in the diode by the transformer turns ratio. Again a rail gap would be justified because of its large electrode area over which to distribute erosion. The switch closure speed is much less critical than in a Marx, so it may be possible to design a diffuse discharge switch with lower erosion rates than a spark channel switch. Current developments in the area of pseudospark switches<sup>3.60</sup> give hope for solutions developing over the next decade. The same amount of erosion would take place in a Marx generator for this job. In a Marx the switches are in series, while in the modulator they are in parallel. In fact, since the switches would be in parallel, we could split the modulator into separate units, each feeding a single transformer via a single switch.

A comparison of PFL parameters for a 1.5 MV pulse power system using Marx-driven water lines and using pulse transformer driven paper-oil cables is given in Table 3.18.

**Table 3.18. Comparison of Water Line Design with Paper-Oil Cable**

	<b>Water Line</b>	<b>Paper-Oil Cable</b>
Inner Radius, a	40 cm	8.6 cm
Outer Radius, b	66 cm	14.2 cm
Energy Stored / Length	10.1 kJ/m	0.43 kJ/m
Length for 600 ns Pulse	10.0 m	48.8 m
Energy Stored / Line	101 kJ	20.9 kJ
Number of Lines for 400 kJ	4 lines	19 cables

In the laser system architecture, we can take advantage of the flexibility of cables to bend them 90° or more and fit the system components closely together. They have restrictions on bend radius, but it is of order 20:1 for turn radius to cable radius; thus, our 14.2 cm cables radius means ~ 3 m radius turns. The cables may be routed to convenient storage trenches or overhead racks. The slow charge time possible with cables means there can be a long cable connecting the modulators and pulse transformers to the cathode + PFL cables (see Fig. 3.75). The modulators for the whole laser driver system may be co-located in a single area, where as the Marx drivers must be distributed and located contiguous to their water lines, as in Fig. 3.74.

**Concluding Remarks on Pulsed Power.** The comparison between energy storage in water and paper-oil dielectrics has been examined to a certain point. An informed decision will require more operational experience. For example, large scale water lines storing up to 100 kJ have never been run at repetition rate, whereas a cable system has been run at 50 Hz at 800 kV charge voltage, although at a relatively low energy of 15 kJ per pulse. The cable system has advantages in architecture flexibility and possibly in reliability, in that it can be charged using a pulse transformer. Cable manufacture is a mature technology, but cable terminations will require further development to become compact and cost competitive. The energy transfer efficiency for the water line system is thought to be about 90% from power at 150 kV DC to power off the diode cathode. For the cable system the efficiency should be better, of order 95%.

#### **3.4.4.2 Electron Beam System**

**Cathode.** Most e-beam driven excimer lasers have been single pulse machines and have used cold cathodes of metal blades, carbon felt, velvet, etc. Unfortunately, this technology is inappropriate for long life repped operation. One issue is that a more uniform emitter such as

carbon felt has a lifetime  $< 10^5$  pulses. In addition, as it ages it develops emission non-uniformities which are transported by the applied B-field to the foil where the high current areas produce localized foil heating. A technology appropriate for repetitive pulse operation is the thermionic cathode. It was used on the EMRLD laser (100 Hz XeF laser for DoD) and in designs for longer running machines. It does require significant power (to maintain the  $\sim 1200^\circ\text{C}$  cathode temperature in the face of radiative heat loss), and it requires advanced thermal engineering. For the high current density required of our fusion amplifiers ( $40 \text{ A/cm}^2$ ), one would need  $> 20 \text{ W/cm}^2$  of thermal power to be supplied (and removed from where it ultimately is absorbed as radiation). This may be compared to  $100 \text{ W/cm}^2$  of average power carried by the e-beam itself ( $600 \text{ kV} \cdot 40 \text{ A/cm}^2 \cdot 0.6 \mu\text{sec} \cdot 7 \text{ Hz} = 100 \text{ W/cm}^2$ ). Obviously for higher rep-rate lasers, the thermionic cathode heater power is less significant. The thermal engineering must cope with keeping a hydrocarbon and moisture free vacuum system at  $< 10^{-6}$  torr while at  $\sim 1200^\circ\text{C}$ . Clearly, ceramic bushings would be required.

In response to these issues, we have introduced a new plasma cathode<sup>3,48</sup> in our KrF laser driver system. A 10 cm x 30 cm version of this cathode has been demonstrated in Textron's laboratory. Key features such as its ability to achieve very high efficiency and have a construction scalable to larger sizes have been shown. The e-beam diode is illustrated in Fig. 3.76.

This technology requires  $< 1 \text{ W/cm}^2$  to operate the plasma and has a currently projected lifetime  $> 10^8$  pulses, based on erosion rates of switch components. In addition, it is a non-closing diode; unlike traditional cold cathodes, it does not have a plasma that closes the anode-cathode gap (AK gap) during the  $0.6 \mu\text{sec}$  pulse. This has several beneficial effects:

- 1) With no change in AK gap, the space charge limited cathode current does not vary. This means we have a constant impedance load, so near perfect impedance matching is possible.
- 2) With constant impedance, we can design for constant voltage and thus optimum deposition uniformity and pulse-to-pulse consistency for the sequence of 6 ns multiplexed pulses traversing the amplifier.
- 3) These features also imply the ability to run at higher current densities for longer times (i.e., higher coulombs/cm<sup>2</sup> than with closing diodes, which had constraints in this area).
- 4) Non-intercepting diode design is possible. With constant  $B_{\text{self}}$  and  $B_{\text{applied}}$ , the electron trajectories are constant. This, together with our ability to make cathodes emit only in areas that map into open areas of the foil supporting "hibachi," means we can have a diode with transmission efficiency limited only by the albedo of the foil(s) and the laser gas (minimized by low atomic number, Z, materials and gases).

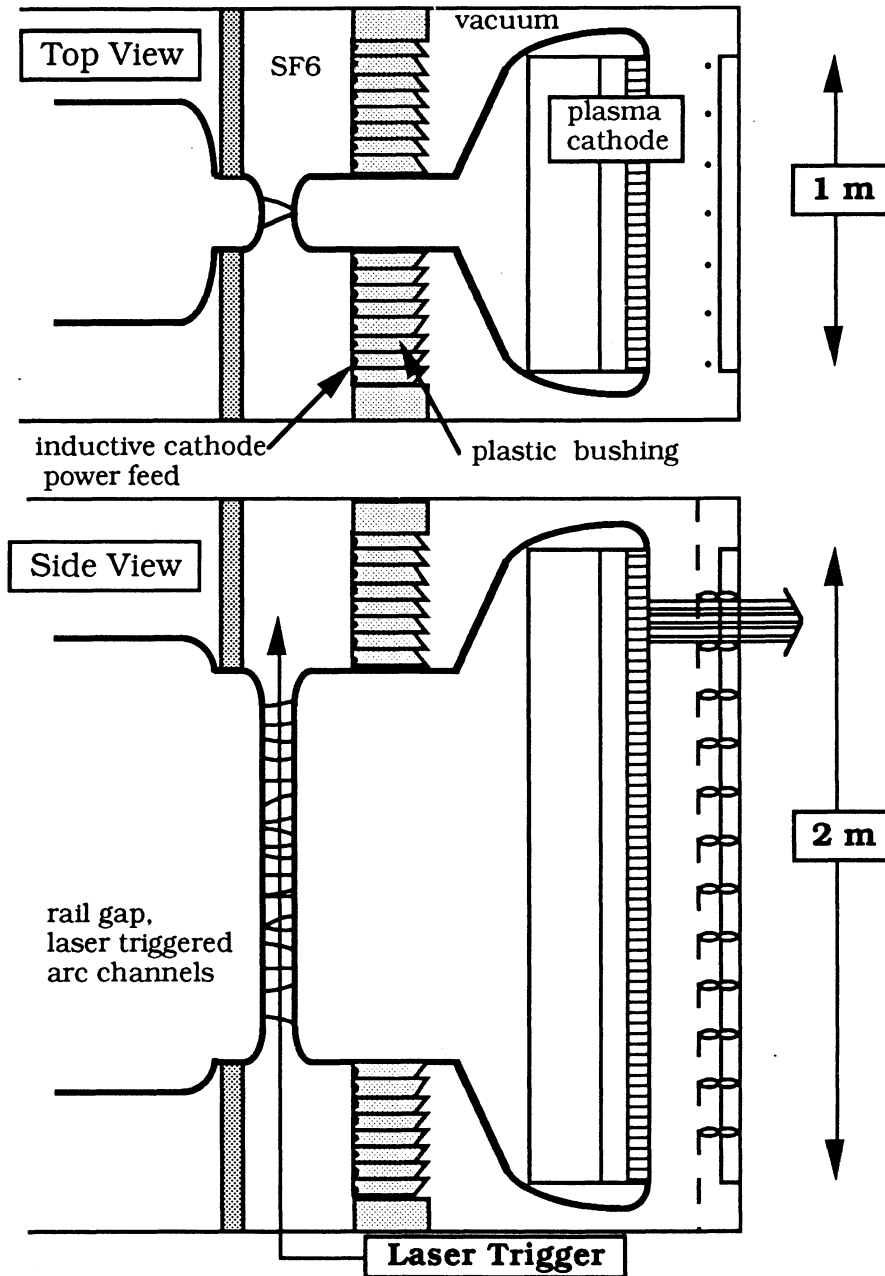


**Fig. 3.76. Top and side views of Textron's electron-beam diode for a 60 kJ amplifier.**

We require in the present design  $40 \text{ A/cm}^2 \cdot 0.6 \text{ } \mu\text{sec} = 24 \text{ } \mu\text{coul/cm}^2$  (plus rise and fall time requirements). In response to a particular DoD program need, our research on this cathode technology has demonstrated  $6 \text{ A/cm}^2$  for  $5 \text{ } \mu\text{sec}$  and  $15 \text{ A/cm}^2$  for  $1.5 \text{ } \mu\text{sec}$ . Operation at  $2 \text{ Hz}$  has been demonstrated;  $10 \text{ Hz}$  should be possible with a small cooling circuit and more efficient use of gas in the plasma. We have operated with applied magnetic fields up to  $2.3 \text{ kG}$ , and our present design should work to over  $4 \text{ kG}$ . Some modification to the design may be necessary for

the 5 to 6 kG needed in the present case. Thus, we are fairly confident of meeting the present design requirements with a reasonable amount of further R&D and demonstration.

The plasma cathode has a power requirement of its own for the low voltage discharges in its structure. This requirement is modest because it operates with about the same current per unit area of cathode face area, but at a voltage of ~ 1.5 kV. Since the e-beam in the present design operates with 600 kV, the plasma cathode power requirement is only 1.5 kV/600 kV = 0.25% of the e-beam power. The average current requirement is

$$J \cdot 1.5\tau vA = 40 \text{ A/cm}^2 \cdot 1.5 \cdot 0.6 \mu\text{sec} \cdot 7 \text{ Hz} \cdot 2 \text{ m}^2 = 5 \text{ A}$$

in the present case (the cathode operation is ~1.5 times longer in duration than the e-Beam). This current is easily carried by a thin wire wound in a bifilar spiral up the bushing structure. The inductance of such a spiral is high enough to give good isolation during the 0.6 μsec pulse. It can also be used to inductively grade the bushing.

The plasma cathode also requires a small puff of low pressure gas into its structure for each pulse; here we examine the gas consumption and pumping speed requirements. Our research versions of the cathode have operated with an input of about 15 gas molecules per electron emitted; we believe there is scope for a large reduction in this ratio to less than one molecule of gas per electron. This will be accomplished by designing for smaller manifold volume in the gas distribution system (i.e. gas release closer to the required discharge volumes). In addition, we would use sorption pumping at LN<sub>2</sub> temperature in the cathode back space where the pressure is 10<sup>-2</sup> torr (as opposed to 5x10<sup>-5</sup> torr in the AK gap). With these improvements the required pumping speed,  $S = J\tau vA / qP_{\text{base}}$ , would then become

$$S = 40 \text{ A/cm}^2 \cdot 0.6 \mu\text{sec} \cdot 7 \text{ Hz} \cdot 2 \text{ m}^2 / (1.6 \times 10^{-19} \text{ coul} \cdot 5 \times 10^{-5} \text{ torr}) = 17,000 \text{ liter/s}$$

This pumping speed represents less than 10% "open wall" pumping speed for one side of the diode.

Relative to simpler cold cathodes, there is more depth required for the structure of the plasma cathode assembly. Based on our present designs, this depth is  $(17 + J\tau 10^6 / 2)$  cm. The first term is composed of 4 cm for the discharge region, 8 cm for the gas distribution region, and 5 cm for switches and controls. Future designs will require less gas distribution depth, as we discussed above, but will require depth for the sorption pump. The term with  $J\tau$  represents energy storage requirements; this depth may reduce by up to two fold for more advanced future energy storage. In summary, the depth requirement is a design consideration, but is not an issue.

As we have mentioned, the non-closing plasma cathode will allow a patterned emission that releases electrons only in areas that map, by the net B-field transport, into open areas of the foil support ribs ("hibachi" structure). We have demonstrated in the laboratory 92% transmission through a fine featured foil support structure; near 100% should be possible for a structure with 2 to 5 cm openings, such as we could use in our KrF amplifiers. Given this, the albedo of the foil-gas combination becomes controlling for the overall e-beam efficiency. In the next section we discuss the foil and foil cooling design.

**Foil.** If we design our foil support structure with 1 inch openings and a support angle of  $25^\circ$ , as shown in Fig. 3.77, and assume titanium foil material (Ti 15-3-3-3), for which we have the best data base for e-beam pumped lasers, with a working peak cyclic stress of 60 ksi at up to  $600^\circ\text{F}$  for  $10^7$  to  $10^9$  cycles,<sup>3.61</sup> then for 1 atm plus 2 atm over pressure, we conclude a thickness of 2.4 mil (0.0024 inch) is required. We have also checked the elongation and find it to be 0.3%, which is less than the 1% allowed. While this is a possible solution, we prefer to believe that good beryllium and beryllium-aluminum foils could be made in the requisite sizes by the time the technology was needed. The advantage is the lower stopping power ( $\sim Z = 4$  for Be, and  $Z = 22$  for Ti); hence, more efficient e-beam transport and lower heating would be achieved. Recently, large width beryllium foils have been manufactured, and some preliminary testing at Textron has shown that they can be used for large span, high pressure, vacuum/gas windows. Pure beryllium is brittle, but beryllium/aluminum alloys with 25% to 40% aluminum have been made and are much less brittle. The strength of the 25% alloy is as good as the pure beryllium, 85 ksi as rolled. We assume the fatigue strength of the 25% alloy is 80% of its tensile strength (the same ratio as for pure beryllium). Thus, we assume 60 ksi for  $10^9$  cycle fatigue at up to  $600^\circ\text{F}$ ; these numbers are comparable to those for Ti 15-3-3-3.

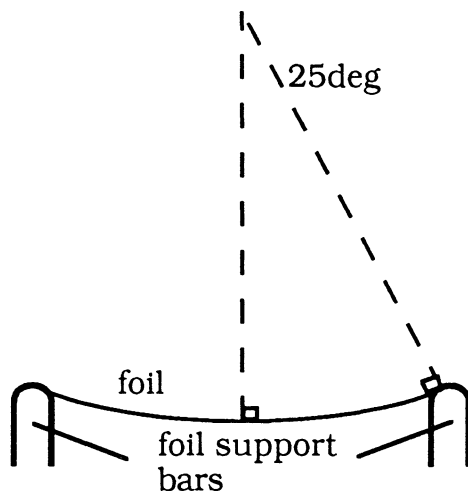


Fig. 3.77. Foil support bars with foil at design support angle of  $25^\circ$ .

Foil heating occurs with each pulse of the e-beam, so a steady state removal of heat is required. For support bar spacings that are relatively large, as is advantageous for non-intercepting design, it is difficult to conduct the heat to a foil support bar, which could have water cooling passage. A better solution, which we have assumed in our design, is to use a double foil system with gaseous helium flowing between the foils for convective heat removal, as shown in Fig. 3.78. We have used a 1-D Monte-Carlo (TIGER) code to calculate the e-beam energy deposition in a dual foil system consisting of 1 mil (= 0.001 inch =  $2.5 \times 10^{-3}$  cm) of Be and 1 mil of Be sandwiched with 1 mil of Al. We include an estimate of the additional energy deposited by electrons reflected by the laser gas; it is a 25 to 35% effect. The average heat load into the Be/Al foil is then  $\delta V J \tau v = 35 \text{ kV} \cdot 40 \text{ A/cm}^2 \cdot 0.6 \text{ } \mu\text{sec} \cdot 7 \text{ Hz} = 5.9 \text{ W/cm}^2$ . The second foil of Be alloy will have a heating rate of  $\sim 2.3 \text{ W/cm}^2$ . The stopping power of 0.5 atm of helium between the two foils is negligible, and thus so is the e-beam heat input. Overall we need to remove  $\sim 5.9 + 2.3 + 0.5$  (from anode wire radiation) or  $\sim 9 \text{ W/cm}^2$ . For the present design, we estimate 300 g/sec of helium for the 2-m-high  $\times$  1-m-wide e-beams on the ultimate amplifiers. The temperature rise in the helium will be  $\sim 120 \text{ }^\circ\text{C}$ . The titanium option would require  $\sim 2.6$  times greater heat removal.

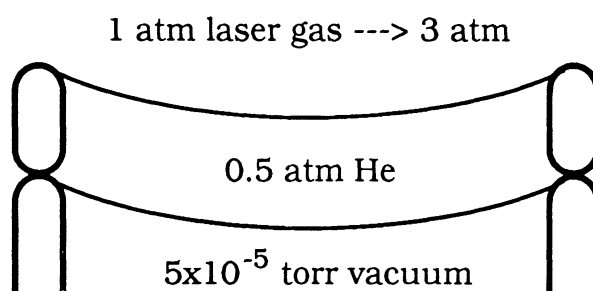


Fig. 3.78. Double foil system with gaseous helium for convective foil cooling.

**Diode Inductance and Rise Time.** We have modeled the diode structure for purposes of determining its inductance, which divided by the impedance determines the rise time  $\tau \approx L/Z$ . In our present 60 kJ design, the rise time is about  $30 \text{ nH} / 0.6 \text{ } \Omega = 50 \text{ ns} = 8\%$  of 600 ns. Larger lasers quickly lose efficiency in this area because inductance grows and impedance decreases with laser size. This of course was quantified at the time we did the amplifier efficiency optimization described in Section 3.4.3.

**Anode.** The anode in the e-beam diode is composed of a plane of parallel wires or filaments. It is desirable to minimize the interception of electrons by the anode and to have it cool

by passive radiation, if possible. We write the equation for the heat input per unit length as  $2aJV\tau\nu$ , where  $a$  is the filament radius,  $J$  the current density,  $V$  the e-beam voltage,  $\tau$  the pulse time, and  $\nu$  the rep-rate. This is balanced by the radiative loss per unit length of  $2\pi\epsilon\sigma T^4$ , where  $\epsilon$  is the emissivity of the wire at temperature  $T$ , and  $\sigma$  is the Stefan-Boltzmann constant. Equating these terms gives

$$T = \left[ \frac{JV\tau\nu}{\pi\epsilon\sigma} \right]^{1/4}$$

For  $J = 40 \text{ A/cm}^2$ ,  $V = 600 \text{ kV}$ ,  $\tau = 0.6 \text{ } \mu\text{sec}$ ,  $\nu = 7 \text{ Hz}$ ,  $\epsilon = 0.5$ , and  $\sigma = 5.7 \times 10^{-12} \text{ W/cm}^2\cdot\text{K}^4$ , we get  $T = 1830 \text{ K}$  or  $1560 \text{ }^\circ\text{C}$ . The anode material could be carbon or tungsten filaments under small tension, since carbon sublimates at  $3700 \text{ }^\circ\text{C}$  and tungsten melts at  $3387^\circ\text{C}$ . The lack of diode closure arcs should allow the anode a long lifetime.

Assuming the anode wires represent a 1% interception, as in 0.25 mm filaments spaced every 2.5 cm (the A-K spacing is  $\sim 5 \text{ cm}$ ), then the heat load per unit of cathode or foil area is  $0.01 \cdot JV\tau\nu = 1 \text{ W/cm}^2$ . Half will go to the cathode (adding to the  $0.7 \text{ W/cm}^2$  cathode plasma/discharge dissipation) to be carried away by the continually pumped out gas, and half will go to the foil system - a contribution already included in the helium cooling load.

**Lifetime Issues.** We list the following lifetime issues:

- 1) Erosion of laser triggered spark-gap electrodes,
- 2) Aging of the foil by e-beam irradiation,
- 3) Chemical attack on the foil by the 0.6% fluorine containing laser mixture,
- 4) Erosion of cathode discharge electrodes,
- 5) Life of discharge commutator in the plasma cathode,
- 6) Life of cathode discharge capacitors,
- 7) Bushing deterioration due to x-rays.

We have examined each of these issues. In general, those components suffering erosion are of most concern when considering  $1.6 \times 10^8$  pulses per year (75% duty at 6.7 Hz). The laser triggered rail gap we estimate would need service once a month if it were of simple fixed construction. On the other hand, if the emitting area is a rotatable rod or cylinder, new surface could be rotated into place via a  $30^\circ$  rotation each month, giving a year of operation before replacement of a part is necessary. The cathode discharge electrodes are estimated to have a 10-year lifetime. Other areas of concern in the cathode have service intervals of a year or longer. Similar concerns occur in the commutator for the cathode discharge current since it carries about the same number of coulombs as the e-beam itself. We propose the use of pseudospark switches

in this area,<sup>3.60</sup> and, again, the principle of designing switches that allows the introduction of new surface material is a design concept that we propose could be developed for this application.

### 3.4.4.3 Flow

The flow loop must provide homogeneous gas with very small density perturbations ( $\delta\rho/\rho$  of order  $10^{-5}$ ) in the laser cavity for each new pulse. It is a closed cycle system, which means that steady state waste heat removal is required, along with acoustic suppression of the over pressure from the e-beam deposition. Figure 3.79 gives representative dimensions for a 60 kJ laser cavity operating at 10 Hz with 1 atm of Ar:Kr = 1:1 at 300 K, with 290 J/liter energy deposition. The over pressure is calculated to be 1.9 atm. With a 2 m cavity in the flow direction, a flush factor of 1.5, and a 10 Hz rep-rate, the flow speed is 30 m/s and Mach number in the cavity, based on initial gas conditions is 0.12. The Reynold's number is  $3.2 \times 10^6$ .

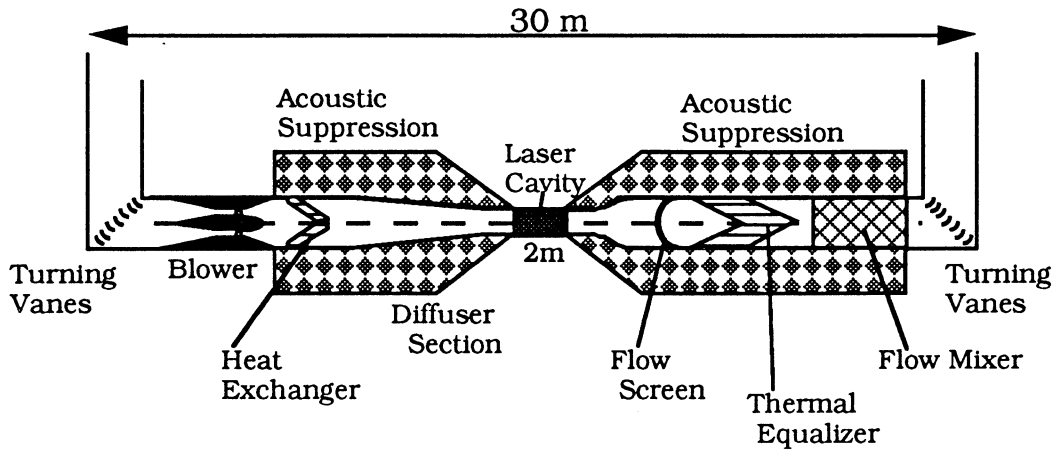


**Fig. 3.79. Flow system for 60 kJ amplifier cavity; flow is from right to left in the figure.**

The design shown was sized based on design approaches developed in the EMRLD program (a DoD high average power, e-beam pumped, XeF excimer laser) and scaling studies done for laser fusion.<sup>3.62</sup> The diffuser operates with a total angle of  $8^\circ$ , expanding the flow area by a factor of three. This area ratio allows the other flow components, such as the heat exchanger, flow mixer, and thermal equalizer, to operate at lower dynamic head by a factor of  $3^2 = 9$ . The pressure drop across the flow hardware (turning vanes, mixer, heat exchanger, and so forth) determines the blower size. This design will require that it supply  $\Delta p$  of about six dynamic heads ( $1/2\rho v^2$ ) of pressure drop, based on  $\rho$  and  $v$  in the laser cavity. Thus,

$$\Delta p \sim 6 \cdot 1/2 \cdot 2.3 \times 10^{-3} \text{ g/cm}^3 \cdot (2000 \text{ cm/sec})^2 \Rightarrow 0.4 \text{ psia.}$$

Clearly, the size of a laser is determined by the flow loop, which is related to the need to suppress acoustic energy between pulses. This is related to total energy deposition, which is proportional to laser energy required for the target. Given that Fig. 3.79 represents what is required for each 60 kJ cavity, and that we need 60 such cavities for 3.6 MJ on target, we could eliminate the 90° turning vanes, shown in the figure, and link 60 such segments into a single circular loop of circumference  $60 \cdot 30 \text{ m} = 1800 \text{ m}$ , or a diameter of 600 m. Perhaps two loops of 300 m diameter or four loops of 150 m diameter would make more sense. These large flow loops could be centered on the SOMBRERO reactor building. These chains of amplifiers would not have to be circular, but could be oval, hexagonal (etc.), serpentine, rectangular, or square. A large number of amplifier cavities in a single flow loop, puts them all at risk if there is trouble with flow loop components of one of them. For this reason, we have settled on the arrangement shown in Fig. 3.80. Fifteen of these flow loops, each with four cavities, will supply the nominal requirements of 3.6 MJ on target. We also include a spare loop with four cavities for speed and ease of supplying the required laser beams while servicing an amplifier.

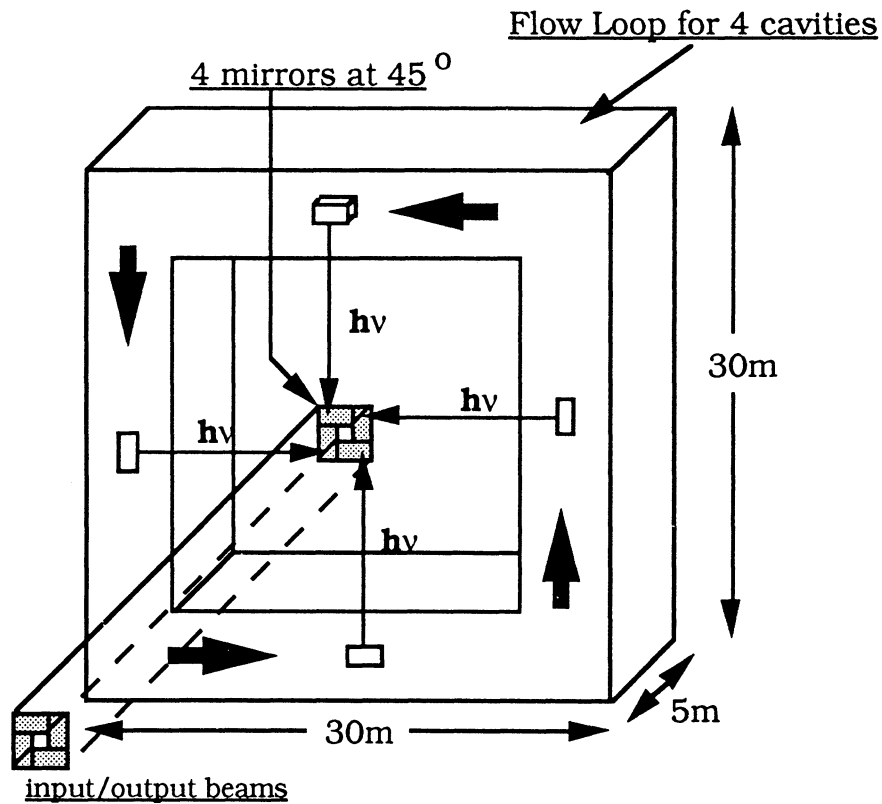


Fig. 3.80. Flow loop with four 60 kJ amplifier cavities.

The cavities in Fig. 3.80 operate as two pass amplifiers. We show in the figure a grouping of four mirrors, at the center of the flow loop, one for each cavity, each at 45° angle to the line of sight to its cavity window and mirror, each of dimensions 1.4 x 2 m (1x2 m projected area at 45°), matching the beam dimensions at the cavity mirror. The individual beams (each 6 ns long) are largest at the cavity mirrors and decrease as they go to the feed arrays. The bundles of beams from/to the feed array require approximately constant cross sectional area. Since we are carrying the beam paths in vacuum from the large amplifiers, there is advantage in packing them together as we turn 90° to transmit from/to the feed arrays.

#### 3.4.4.4 Optics

Short pulse (~ 6 ns) optics are assumed to operate with loadings of 5 J/cm<sup>2</sup>. This is the same fluence as was assumed for the more near term LMF single pulse KrF laser fusion experimental facility.<sup>3.63</sup> It is difficult to know what is truly credible for 1.6 × 10<sup>8</sup> pulses per year. We note that good progress has been made in damage limit improvement in recent times, and this application is for tenth of a kind in the year 2040. Recently, damage values as high as 28 J/cm<sup>2</sup> were reported for laser annealed, multi-layer coated optics operating at 248 nm with 15 ns pulses.<sup>3.64</sup> We de-rate from this in our system design to account for shorter pulse lengths, non-uniformities in the fluence, including those from diffractive effects, long term repetitive operation, and to account for non-uniformities in coating manufacture and performance.

The steady state heat load for repped operation is ~ 5 J/cm<sup>2</sup> · 7 Hz · 0.1% absorption = 0.035 W/cm<sup>2</sup>. This is a modest load that may be removed by cooling passages in the substrate.

**Propagation.** Long path beam propagation of 248 nm in the atmosphere is an issue for several reasons. They include Rayleigh, aerosol, and Raman scattering, the absorption by atmospheric gases (especially by ozone), and phase front distortion by density fluctuations and gradients caused by thermal eddys and thermal gradients. These issues are discussed by Rosocha et al. for the Aurora system.<sup>3.65</sup> We add to that discussion by noting that for an IFE driver the total path lengths are larger, of order 1 km and more, thus exacerbating the problems. In addition, the broad band width of KrF fluorescence means that there is already radiation at the N<sub>2</sub> S(8) Raman wavelength (76 cm<sup>-1</sup> shift) to seed the Raman transition. The Raman gain is ~1 cm<sup>2</sup>MW<sup>-1</sup>km<sup>-1</sup>. The short pulse beamlets get up to 5 J/cm<sup>2</sup>/6 ns ≈ 1 GW/cm<sup>2</sup>, so gains of several decades occur in 10's of meters and one has self seeding. It seems likely that multiple uncontrolled Raman shifts would occur. Thus it is clear that an optically inert gas or a vacuum should be used for the long beam paths.

The advantage of a gas medium at 1 atm, as opposed to vacuum, is that the ducting does not have to hold off an atmosphere of pressure. On the other hand one does need a scheme for

introducing the gas, while displacing the air without mixing, in a system of interconnected paths, elbows and T's. In addition, the walls must be multiply insulated because the fluctuations need to be of order  $\delta\rho/\rho = 3 \times 10^{-5}$  or less (i.e.  $\delta T < 0.01^\circ\text{K}$ ) if the path lengths are of kilometer scale. This is true even if the gas is helium (the best possible optical choice) and the density non-uniformities transverse to the beams are disordered.

Vacuum is our choice because the architecture we have developed consolidates beam lines and makes cylindrical vacuum ducts practical and of reasonable cost. With vacuum we eliminate any uncertainties related to the propagation medium.

#### **3.4.4.5 Magnetic Field Coils**

A pair of coils is required to produce an applied magnetic field, parallel to the e-beam direction, of magnitude ~3 times the self field from the e-beam current flow in the diode. The self field for our nominal design is ~1.75 kG, so our applied field should be ~ 6 kG. The rectangular coil dimensions are roughly 2 m x 3 m spaced by 1.5 m. They require  $\sim 10^6$  amp-turns to produce the desired field at the center of the pair.

We assumed NbTi superconductor at 6.2 K, which allows 2<sup>o</sup> margin for pool boiling of helium. The current density was taken at about 200 kA/cm<sup>2</sup> for each of the two coils, which includes a 2x safety margin for the superconducting operation. The copper stabilizer is designed for 3200 A/cm<sup>2</sup>, which is very conservative.

#### **3.4.4.6 Controls**

We made an estimate of the controls required for each e-beam, pulse power system, flow loop and mirror system. We assumed the need for a large number of sensors per unit to ensure the ability to keep continuous intelligence about developing maintenance needs. For example, for each e-beam we have a total of 23 sensors, for each e-beam pulse power system - 40 sensors, for each flow loop - 12 sensors. We included control rooms and displays.

### **3.4.5 System Architecture**

#### **3.4.5.1 Ultimate and Penultimate Amplifier Layout**

Given the module shown in Fig. 3.80, and the symmetric irradiation requirements of 60 directions uniformly spread over  $4\pi$  steradians, one can draw an architecture with a group of four flow loops, each having four 60 kJ cavities, on each of four sides, call them north, south, east, and west. This gives one flow loop with four cavities as a spare for system redundancy. The west side lasers are shown with a 100 m diameter SOMBRERO reactor building in Fig. 3.81. By symmetry one can visualize the other three sides.

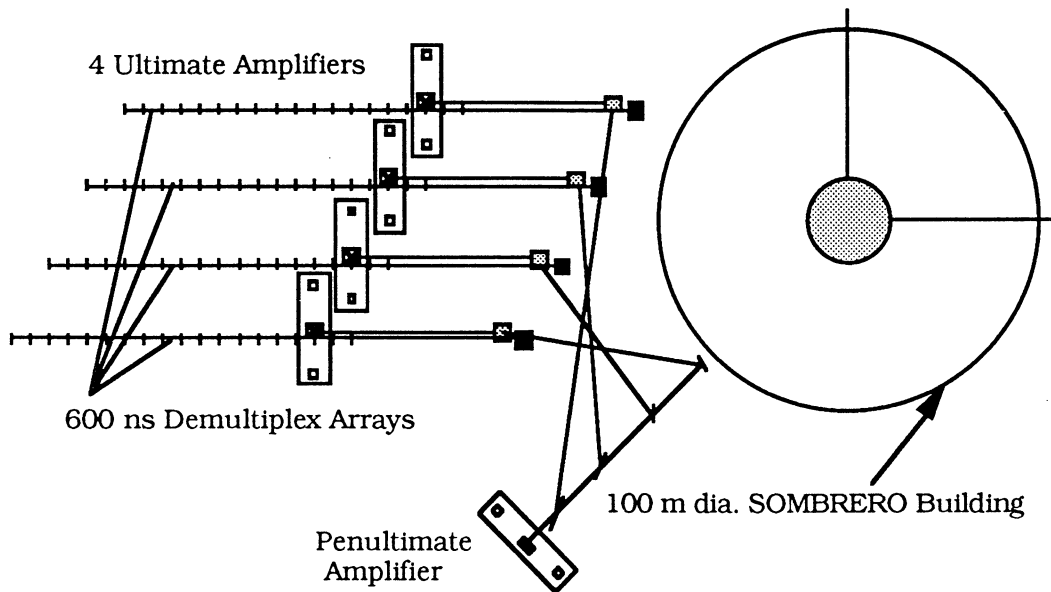


**Fig. 3.81. One fourth of a laser driver system in an architecture spreading the lasers uniformly around the SOMBRERO building; four flow loops, each with four 60 kJ amplifier cavities, and their associated 600 ns demultiplexing arrays, are shown as well as the preceding stage Penultimate amplifier.**

This architecture has two difficulties. There is need for room on the east and the south sides for various balance of plant equipment to be located. In addition, one desires to compact the laser system to minimize building costs. Our desire to carry the beam lines in vacuum, or in high thermal uniformity helium, calls for a design that brings beam lines together as much as possible. Figure 3.82 shows an architecture that responds to these constraints.

In Fig. 3.82 the total system is split into two equal parts located on the north and west sides. On the north side we label the input/output array for the thirty-two 60 kJ amplifier cavities housed in 8 flow loops. On the west side we show a representative optical path of a single 6 ns beam leaving its 2x4 cm feed mirror, going north to a 45° turning flat, going east to a next 45° turning flat, then going north to the turning flat in the center of the flow loop, discussed for Fig. 3.80, and then going into the appropriate one of the four 60 kJ cavities of this flow loop. One of these 6 ns pulses gets amplified to energy  $\sim 60 \text{ kJ}/100 = 600 \text{ J}$  since we have multiplexed the 600 ns amplifiers to one hundred 6 ns beamlets. Thus, after a double pass transit of the amplifier, the beamlet follows an angularly offset path back to the input/array where it is picked up on an 8x16 cm mirror which recollimates it and sends it west to the demultiplex array. The demultiplex array provides a designed time delay, and then sends the beam on to the beam handling area under the SOMBRERO building.

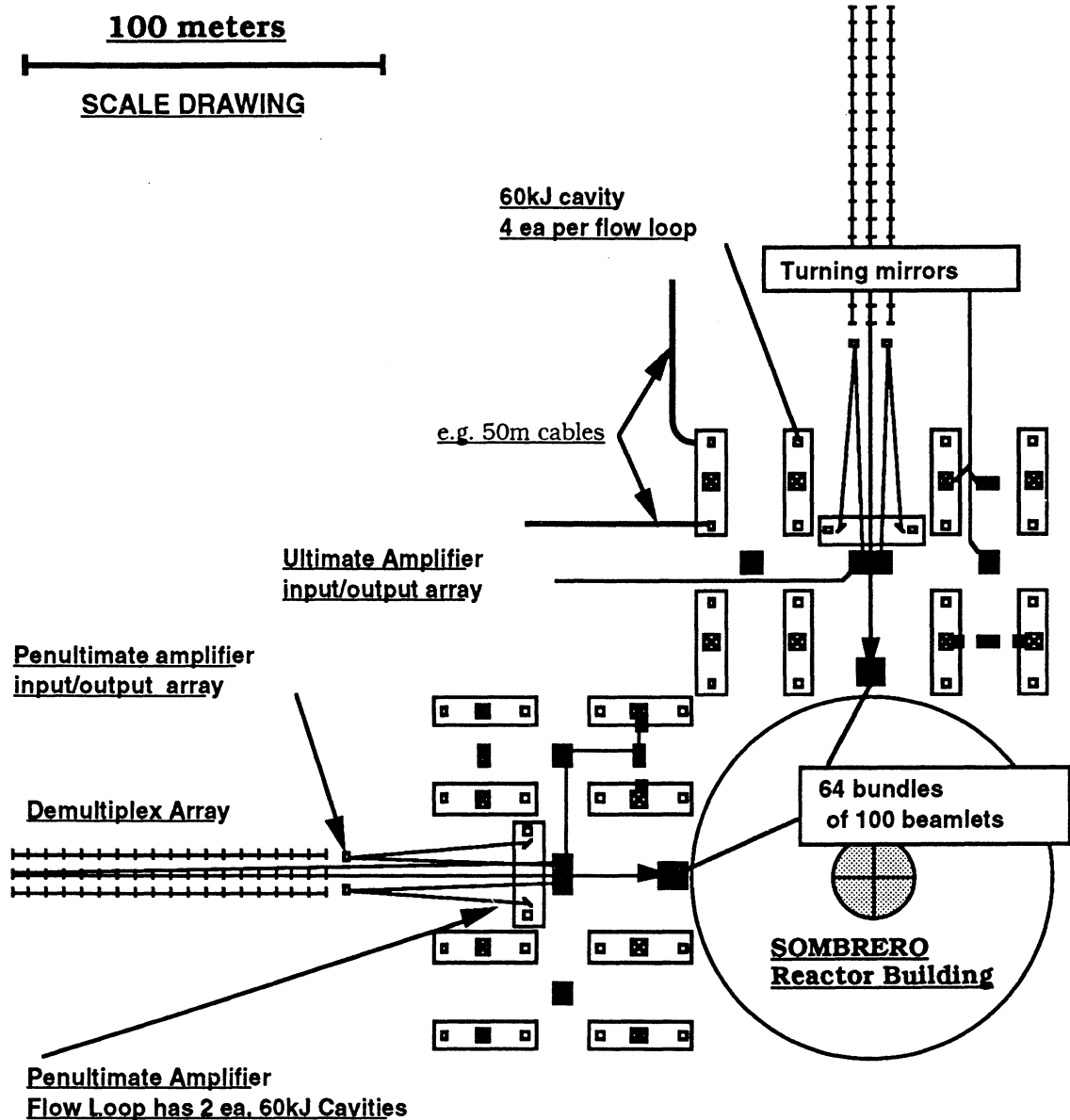


Fig. 3.82. Architecture for Ultimate and Penultimate amplifiers.

There are two penultimate amplifier flow loops, each with two 60 kJ cavities, located on the west and north sides, respectively. The counting is clear since the ratio of 64 ultimate amplifier cavities divided by their Gain = 16 implies 4 penultimate cavities of the same energy output. There are some optical losses between stages obviously, but we are not considering this at this stage of conceptual design. The penultimate amplifiers can be in flow loops identical to those of the ultimate amplifiers, but with two sides vacant of amplifier cavities. However, we would have cavities in three sides to give redundancy at this stage of the amplifier chain. The extra cavity would have flow continuously going through it and its blower operating, but would not be e-beam pumped unless needed, at which time mirrors would redirect beams to the standby cavity.

The total number of 6 ns beamlets is  $64 \cdot 100 = 6400$ . 6,000 of these are active at any time and are distributed into 60 directions onto the target. The directions are sorted in the beam handling area under the SOMBRERO building. If the beams go the most direct route possible, there are different path lengths to the target for each of the 60 directions. Appropriate time delays may be introduced via optical "trombones" in this area and/or by use of the demultiplex array trombones. Use of the extra four laser cavities when needed will require them being able to supply any of the 60 directions, which will call for special trombones and mirror insertion possibilities in the design.

Figure 3.82 shows to scale, schematically, pulse power cables of the requisite ~50 m length, with 3 m radius turns, which can be used to bring them to a suitable rack or trench. The modulators and pulse transformers may be located in a building on the NW corner, between the two systems.

As mentioned in Section 3.4.3 on amplifier optimization, we will use interleaved input/output arrays. For our amplifier  $h/w = 2$  window aspect ratio, we use mirrors with aspect ratio two. The geometry of the interleaved arrays is illustrated in Fig. 3.83. Starting in the upper left, we see a  $2 \times 4$  cm mirror that feeds energy ( $600 \text{ J} / 16 = 38 \text{ J}$  in 6 ns), by way of 3-fold

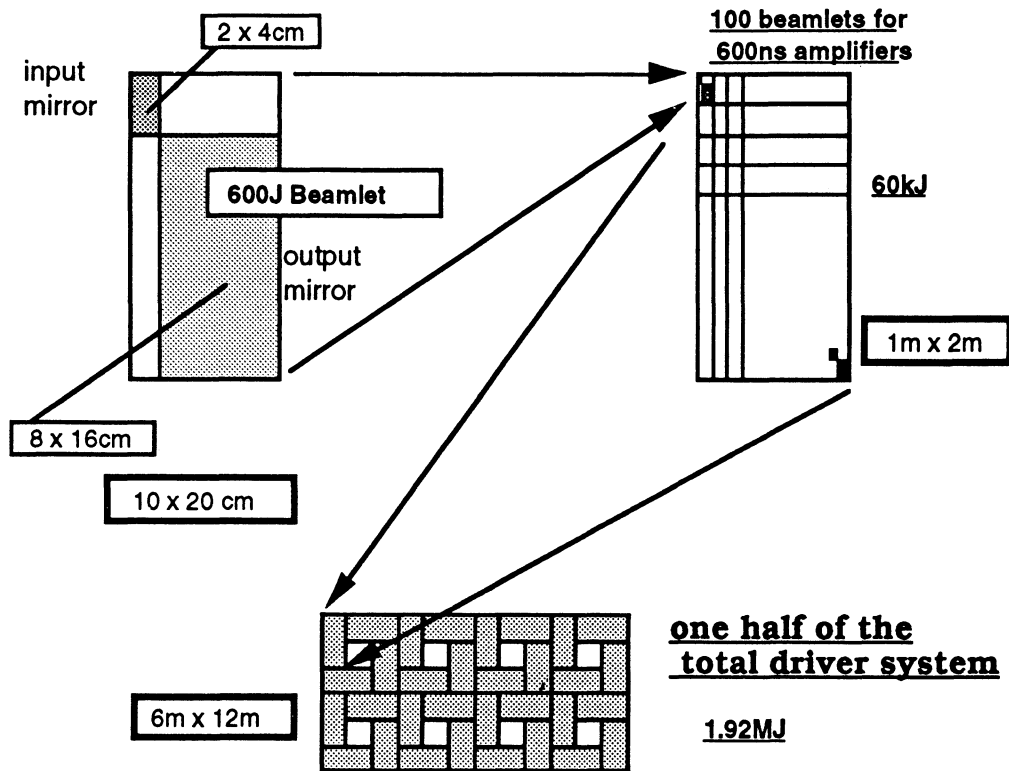


**Fig. 3.83. Interleaved mirror arrays for input / output to the 60 kJ Ultimate Amplifiers.**

mirrors, into one of the 60 kJ cavities where in a 2-pass transit it is amplified to 600 J and is picked up, after 3-fold mirror reflections, by an  $8 \times 16$  cm output mirror. The pickup mirror is not the one adjacent to the input mirror but is equal distance diagonally across the center of the array of 100 input mirrors interleaved with 100 output mirrors. One of these arrays is shown schematically in the upper right of Fig. 3.83. Finally, 32 of these arrays of 100 input/output mirrors are grouped as shown in the bottom of Fig. 3.83.

### 3.4.5.2 Intermediate Stages

There are a number of architectures that may precede the Penultimate and the Ultimate amplifier stages. We list in Table 3.19 a possible set of prior stage specifications for illustration.

**Table 3.19. System Amplifier Sequence**

<b>Stage</b>	<b>Total Energy</b>	<b># Amp's + Spares</b>	<b>Cavity Energy</b>	<b>Amp Gain</b>	<b>Extraction Time</b>	<b>Total # of Beamlets</b>
Ultimate	3,600 kJ	60 + 4	60 kJ	16	600 ns	6,000
Penultimate	240 kJ	4 + 2	60 kJ	16	600 ns	400
AntePenU...	20 kJ	1 + 1	20 kJ	20	600 ns	100
PreAntePenU..	1.4 kJ	1 + 1	1.4 kJ	25	150 ns	25

### 3.4.5.3 Front End

The front end for the system has several requirements. We desire broad band KrF emission ( $\Delta v/v \sim 0.1\%$ ). This is consistent with the natural fluorescence bandwidth of KrF so that the approach such as NRL<sup>3.66</sup> has developed, for running KrF itself as a broadband, spatially incoherent initial source is suitable. In addition, we note that the de facto target gain is considerably enhanced if the individual beams which illuminate the target reduce their diameter at the target, as the target implodes, by a factor of two in diameter during the  $\sim 6$  ns of the most intense part of the illumination (the remainder of the implosion occurs after this). This is referred to as the "zooming" front-end option. For the overall system design that is appropriate for non-echelon ISI direct drive target illumination, this approach leads to easily understood front end requirements. The entire laser system images the front-end aperture onto the target, with amplification at the spatial Fourier transform of the front-end aperture. If one needs a two times smaller spot on the target, then a two times smaller aperture at the front-end source is required. Unfortunately one will need the same amount of power (watts, not watts/cm<sup>2</sup>) through the variable size aperture in order to extract the same amount of energy from each of the amplifier stages. It

seems possible one could design an electro-optical controlled aperture whose diameter vs time,  $d = d(t)$ , can be controlled in a programmed way during the  $\sim 6$  ns illumination. It would then need to be coupled to a source whose  $W/cm^2$  was  $\sim 1/d(t)^2$ . Alternatively, and easily conceivable with present day technology, is an approach in which  $d = d(t)$  is approximated by stepwise changes in diameter. It would be a matter for target physics calculations to project target gain under the assumption of optimized 2, 3, 4, etc. step changes in spot size; it may be that as few as two or three sizes achieves most of the benefit. For step changes in spot diameter at constant power, we propose a system using a "switchyard," based on pockel cells, in which different front end sources are successively made the origin of the whole KrF driver system. What may seem large and expensive for the amount of energy generated at this point ( $\sim 0.1$  to 1 J) is insignificant in the context of the total system.

Figure 3.84 illustrates a concept using pockel cells and polarized light to provide four different aperture sizes during the pulse. The four "lasers" are operated as broad band sources with uniform emission over their aperture

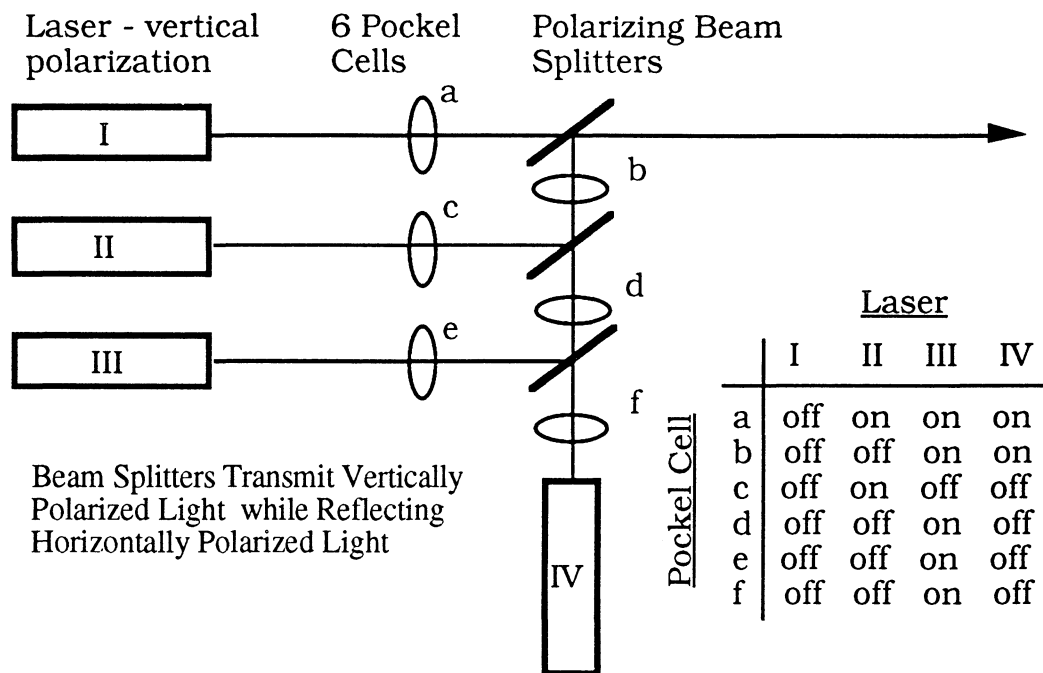


**Fig. 3.84. Pockel cell based "switch yard" to provide four different aperture sizes to image on the target during the  $\sim 6$  ns irradiation.**

### 3.4.6 Grazing Incidence Metal Mirrors

Grazing incidence metal mirrors (GIMM) were first analyzed as a solution to the problem of neutron damage to final optics in 1991.<sup>3,45</sup> This section of the report will summarize important requirements and critical issues for final focusing systems using GIMM. The reader is referred to the original paper for a more detailed analysis.

#### 3.4.6.1 Requirements for Protecting Sensitive Optics

Any beam-line element which is not shielded from the target must be protected from target debris, x-rays, and neutrons. Fortunately, the high-energy x-rays which come from the target can be stopped by the xenon gas that fills the chamber and reactor building. The target debris will either be stopped by the gas (our base assumption) or by a high-speed shutter in the beam line. Shielding optics from neutrons is a much more difficult problem. Neutrons leaving the target move at relativistic speeds and can not be intercepted by a high-speed shutter, and any element which will stop a 14 MeV neutron will not be transparent to a short wavelength laser.

Neutron radiation can destroy dielectric mirrors in three ways:

- degrading the optical transmission of the dielectric materials,
- chemical decomposition of the dielectric materials, and
- destroying the interfaces between dielectric layers.

Transmission degradation data is sparse, and the damage may be removable through continuous annealing. Measurements for MgF<sub>2</sub> and ZnS show an order of magnitude decrease in transmission after 10<sup>16</sup> neutrons/cm<sup>2</sup> (or about an hour of operation for an unshielded dielectric 50 m from a 1000 MWe reactor). Chemical decomposition is a critical issue for all dielectrics. All ionics will undergo significant radiolysis after energy depositions of about 1 eV/atom. Energy deposition of a few eV/atom will also cause significant amorphization in SiO<sub>2</sub>. Chemical mixing at the interfaces of dielectric layers may be the most difficult damage issue to avoid. Any collisional cascade at an interface will cause mixing of the two dielectrics and create a thin, possibly amorphous, region with unknown optical properties. Collisional mixing at the interfaces will occur over a thickness of roughly 3 nm/(DPA)<sup>1/2</sup> (1 DPA, or displacement per atom, corresponds to roughly 10<sup>20</sup> 14 MeV neutrons/cm<sup>2</sup> for most dielectrics), and enhanced diffusion will cause mixing over a thickness 10 times the collisional mixing distances. If the existence of a third phase does not destroy the optical properties of a multilayer mirror, a change of layer thickness of  $\lambda/16$ , or about 20 nm, will destroy the constructive interference used by a  $\lambda/4$  mirror. Under the most optimistic assumptions, it seems highly unlikely that an unshielded dielectric mirror will last more than a fraction of a full power year.

### 3.4.6.2 Design of an Optical Protection System using GIMM

Grazing incidence mirrors can protect more sensitive optics by removing them from the line-of-sight for target neutrons. Figure 3.85 shows a schematic of the final elements of a laser driver. Two layers of shielding represent the chamber and surrounding concrete wall. These will remove almost all of the neutrons which are not coming directly down the beam line. In the SOMBRERO design, the entire reactor building is filled with low-pressure xenon so further protection from x-rays is not needed. The grazing incidence mirror deflects the beam by a few degrees, but will deflect only a small fraction of lower energy neutrons towards the dielectric mirror. Because most of the high-energy neutrons coming directly from the target will pass through the grazing-incidence mirror, a neutron dump or "get-lost hole" placed behind the GIMM can greatly reduce the scattered neutron flux in the rest of the reactor building. In our design, the GIMM is located 30 m from the target, and the final turning mirror is 50 m from the target (i.e., about 20 m behind the GIMM). An analysis of neutron damage to optical elements is given in Section 3.2.5.

### 3.4.6.3 Damage Limits for GIMM

The reflectivity of a conducting metal is a function of the wavelength and polarization of the incident light and the angle at which the light strikes the surface of the metal. If we orient the GIMM so that the incident light has the polarization (transverse electric) which gives the highest reflectivity, the reflectivity of an undamaged aluminum alloy (Al 7475) mirror with an angle of incidence for the light of  $85^\circ$  will be 99.3%. Neutron damage can lower this reflectivity by increasing the resistivity of the metal by introducing defects, transmutations, and surface roughening on an atomic scale (giving an increase in absorptance from the anomalous skin effect), and by introducing microscopic surface roughening which increases the absorptance of the mirror. Based on limited information, we assume that neutron damage will lower the  $85^\circ$  angle of incidence reflectivity to 98.9%. At this reflectivity, thermal stress limits the maximum beam energy intensity to  $1.88 \text{ J/cm}^2$  for a 10 ns pulse. This damage limit sets the minimum required mirror area for a uniform beam. Heat removal requirements will be on the order of 1% of this number, or  $0.02 \text{ J/cm}^2$  per shot.

If damage to the mirror surface can be prevented, the lifetime of the GIMM will be limited by mirror deformation from swelling and creep which lead to defocusing of the beam. Because the defocusing limits for swelling and creep depend on relative fluxes, the limits depend on the longest dimension of the mirror. Longer GIMM lifetimes can thus be obtained by using elongated beams.

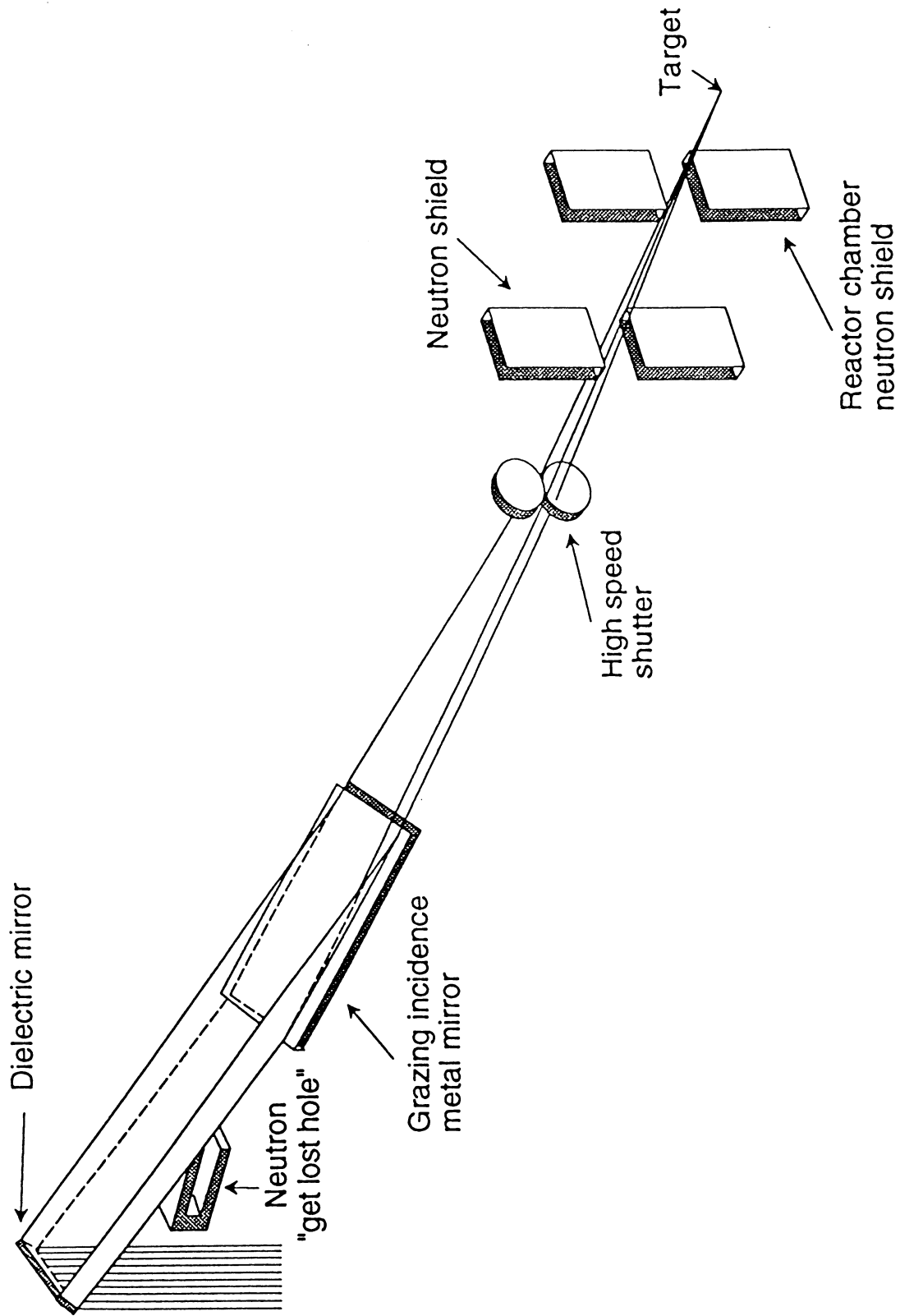


Fig. 3.85 Schematic of focusing scheme using grazing incident metal mirrors.

#### 3.4.6.4 Required Mirror Sizes for Different Grazing Angles

There are two limits on the mirror size. The mirror must be large enough so that the absorbed energy is below the damage limit for the mirror (discussed above), and the mirror must have dimensions that are equal to the beam cross-section for the angle of incidence chosen. If the grazing angle,  $\theta_g$ , is defined as  $90^\circ$  minus the angle of incidence, the second constraint will give the mirror area as the normal-incidence beam cross section divided by  $\sin\theta_g$ . As long as the mirror area calculated from the beam cross-section is large enough to give incident beam energies below the damage limit, the design is workable, but the smaller mirror area can be achieved by adjusting the angle of incidence or the aspect ratio (width / height) of the beam so that the GIMM is operating at both limits.

At small grazing angles, the reflectivity decreases linearly with increasing grazing angle. The damage limit is determined by the absorbed energy, so for small grazing angles, the limit on the beam energy intensity ( $I_{\text{beam}}$ ) at the GIMM can be approximated by scaling the damaged reflectivity with the undamaged reflectivity

$$I_{\text{beam}} = 1.88 \text{ J/cm}^2 \cdot \frac{5^\circ}{\theta_g}$$

This is not exactly correct, since the undamaged absorptance has a small term independent of  $\theta_g$ , but it will be a good approximation for angles near  $5^\circ$ . The minimum GIMM area based on the intensity limit,  $A_I$ , will then be given by

$$A_I = \frac{E}{1.88 \text{ J/cm}^2} \cdot \frac{\theta_g}{5^\circ}$$

Figure 3.86 shows both the required mirror area based on the above constraint and the mirror area based on the beam geometry (beam cross section divided by  $\sin\theta_g$ ). The minimum mirror area is about  $4.1 \text{ m}^2$  and occurs at a grazing angle of about  $6^\circ$ . For this figure, we have assumed the beam cross section area at 50 m is  $(60 \text{ kJ}) / (5 \text{ J/cm}^2) = 1.2 \text{ m}^2$ ; therefore, at the GIMM (30 m from the target) the normal cross-section is  $0.43 \text{ m}^2$ . For a beam aspect ratio of 1, a  $6^\circ$  grazing angle will give mirror dimensions of 6.3 m by 0.66 m. Changing the aspect ratio to 2.3 to 1 gives a mirror size of 4.1 m by 1.0 m. Because non-uniform swelling limits are worse for longer mirrors, and because polishing and support are easier for shorter mirrors, we adopt the 4.1 m by 1 m mirror with a  $6^\circ$  grazing angle as our base design.

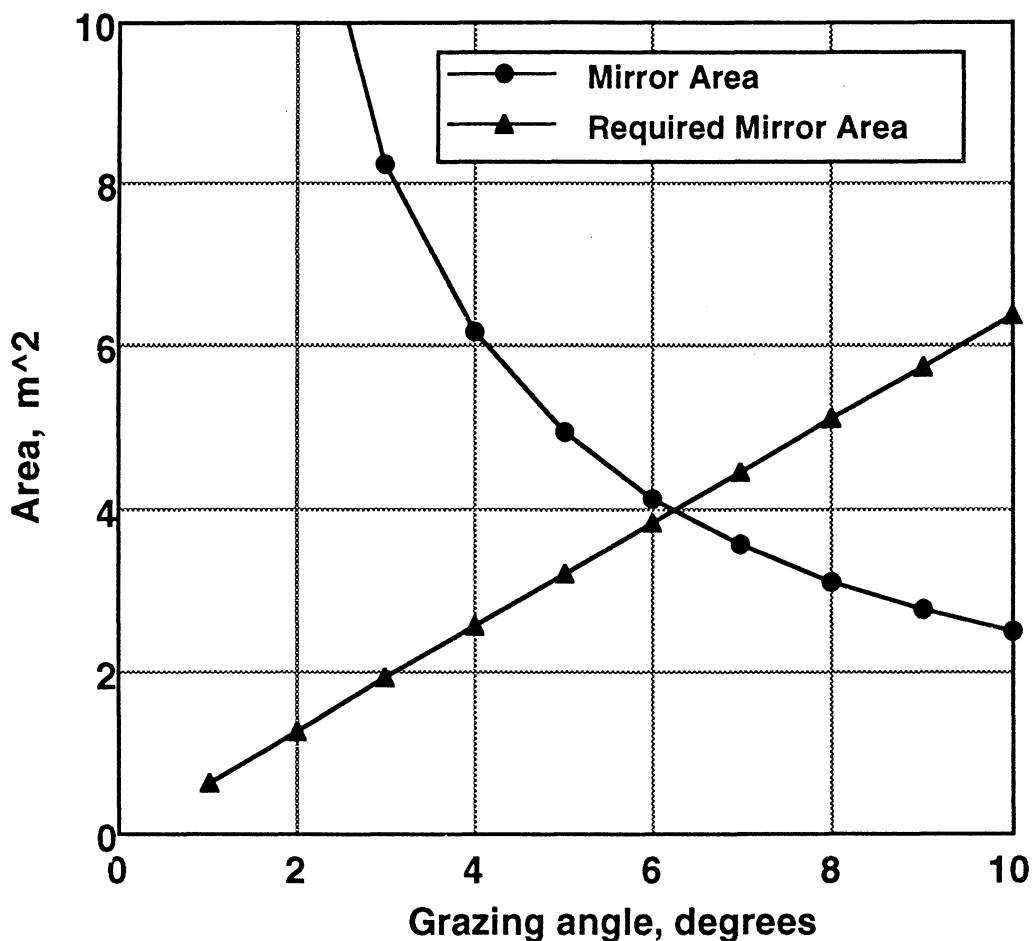


Fig. 3.86. Mirror area based on beam geometry and mirror area required to keep the energy intensity below the damage limit based on thermal stress.

#### 3.4.6.5 Critical Issues for GIMM Use and Survival

Grazing incidence metal mirrors have the potential to solve a critical problem for laser drivers. The most important issues that need to be addressed to assure their integrity include:

- Experimental verification of laser damage thresholds for unirradiated and irradiated mirrors.
- Protection of the GIMM surface from damage or contamination.

A particle or surface defect on the mirror surface will be exposed to the full, normal incidence, beam intensity and could cause explosive "pitting" of the mirror surface. Accumulation of material from the reaction chamber on the mirror surface must be prevented. It may be necessary to have a cleaning system that removes surface

contaminants between shots. A lower energy beam used between shots could be used to vaporize contaminants without explosive "pitting".

- **Beam uniformity studies.**  
Transverse heat flow and stress release during a 10 ns pulse can only average out nonuniformities over distances of a micron or less. Peaks in beam intensity which are wider than a micron could lead to local failure unless the beam is enlarged enough to lower the peak power below the damage threshold. Therefore, if the peak-to-average power ratio is large, the final requirement on mirror sizes may be larger than previously calculated .
- **Beam pointing requirements and mirror support.**  
Moving one end of a 5 m long mirror by only half of a millimeter will move the beam center 1 cm from the target. If the allowed deviation from a perfect plane is limited to  $\lambda/4$ , the limits on local distortions is less than 100 nm.

### 3.4.7 Technology Development Requirements

In Table 3.20, we list major R & D requirements on the path to developing a full scale IFE laser driver system. We also note that in most areas of importance there are alternate technical paths available. Lifetime testing all critical components is clearly required.

**Table 3.20. Technology Development Requirements**

---

<b>Main Amplifier Technology</b>
<ul style="list-style-type: none"><li>• High current density, 600 ns plasma cathode w/ sorption pumping</li><li>• Cable terminations of compact, low cost design</li><li>• Cable for required impedance and voltage w/ optimum insulation for energy storage</li><li>• Dual foil with helium cooling</li><li>• Race track bushing in size required</li><li>• Laser triggered rail gap output switch</li><li>• e-beam demonstration, 1 m × 2 m, 7 Hz, 20 min</li><li>• Flow loop demonstration</li><li>• 60 kJ module demonstration as an oscillator, 7 Hz, 20 min.</li><li>• 60 kJ, rep-rated, angular multiplexed, laser system, 7 Hz, required pulse shape, delivered to diagnostics at a representative target location ...</li><li>• 4 x 60 kJ prototype (square perimeter flow loop); 1 month, 7 Hz operation</li></ul>
<b>Other System Issues</b>
<ul style="list-style-type: none"><li>• Front -End: demonstrate zooming, spatial, temporal and spectral requirements</li><li>• Laser Physics: demo. high <math>\eta</math> at high J/liter</li><li>• Optical coating damage limits for sizes required, with spatial and temporal pulse shapes per system design requirements</li><li>• Final Focus mirror coatings: neutron damage</li><li>• Grazing incidence mirrors: neutron damage and optical J/cm<sup>2</sup> and absorption</li><li>• Be/Al alloy foils for e-beams</li></ul>

---

### 3.8 REFERENCES FOR CHAPTER 3

- 3.1 Y. Gohar et al., "U.S. Solid Breeder Design for ITER," *Fusion Technol.*, **19**, 1538 (1991).
- 3.2 F. Najmabadi et al., "The ARIES-I Tokamak Reactor Study," *Fusion Technol.*, **19**, 783 (1991).
- 3.3 D.K. Sze et al., "Gravity Circulated Blanket Design for a Tokamak Fusion Reactor," Proc. 2nd Topical Meeting on the Technology of Controlled Nuclear Fusion, Richland, WA (1976).
- 3.4 R.W. Conn et al., "SOLASE - A Conceptual Laser Fusion Reactor Design," UWFD-220, Fusion Research Program, Nuclear Engineering Dept., Univ. of Wisconsin, Madison (Dec. 1977).
- 3.5 H.T. Buscher, R.G. Tomlinson, and E.K. Damon, "Frequency Dependence of Optically Induced Gas Breakdown," *Phys. Rev. Lett.*, **15**, 847 (1965).
- 3.6 R.E. Palmer, J.P. Anthes and M.A. Palmer, "The Effect of Background Gas on the Propagation of a High-Intensity Laser Beam to a Target," 1980 IEEE/OSA CLEOS Meeting, San Diego, CA, (February 26-28, 1980).
- 3.7 J.A. Stamper, B.H. Ripin, R.E. Peterkin, Jr., and R. F. Stellingwerf, "Aneurisms in Laser-Driven Blast Waves," *Phys. Fluids*, **31**, 3353 (1988).
- 3.8 R.R. Peterson, J.J. MacFarlane, and G.A. Moses, "CONRAD - A Combined Hydrodynamic-Condensation/Vaporization Computer Code," University of Wisconsin Fusion Technology Institute Report UWFD-670 (July 1988).
- 3.9 J.J. MacFarlane, "IONMIX - A Code for Computing the Equation of State and Radiative Properties of LTE and Non-LTE Plasmas," University of Wisconsin Fusion Technology Institute Report UWFD-750 (December 1987).
- 3.10 "T-4 Handbook of Material Properties Data, Vol. 1c: Equations of State," Los Alamos National Laboratory Report LA-10160-MS (November, 1984).
- 3.11 "Structural Properties of Multidimensional Composites," Southern Research Institute, Presented at the Workshop on CMC's for Structural Applications in Fusion Reactors, Santa Barbara, CA (21-22 May 1990).
- 3.12 R.H. Jones, C. H. Haneger, Jr. And G. W. Hollenberg, "Composite Materials for Fusion Applications," PNL, Richland, Wash., 5th International Conference on Fusion Reactor Materials, Clearwater, Florida (Nov. 17-21, 1991).
- 3.13 R.F. Mattas, "Properties of Bulk Graphical N3M Nuclear Graphite," Argonne National Laboratory.
- 3.14 K. Noda et al., "Summary Report for the ITER Specialists Meeting on Blanket Materials Data Base," Garching, FRG (7-9 Feb. 1990).
- 3.15 D.J. Suiter, "Lithium Based Oxide Ceramics for Tritium Breeding Applications," McDonnell Douglas, MDC E2677 (1983).

- 3.16 *Materials Handbook for Fusion Energy Systems*, Handford Engineering and Development Laboratory, DOE/TIC-10122 (1980).
- 3.17 T. Takahachi and T. Kikuchi, "Porosity Dependence on Thermal Diffusivity and Thermal Conductivity of  $\text{Li}_2\text{O}$  from 200°C - 900°C," *J. Nucl. Mat.*, **91** (1980).
- 3.18 J. S. Botterill, *Fluid-Bed Heat Transfer*, Academic Press (1975).
- 3.19 H.S. Mickley and D. F. Fairbanks, *A.I.Ch.E.J.*, **1**, 374 (1955).
- 3.20 B.V. Berg, A. P. Baskakov, *Khim. Prom.*, **43**, 439 (1961).
- 3.21 A.P. Baskakov, *Inzh. Fiz. Zh. Akad. Nauk. Belorussk.*, **6**, 20 (1963).
- 3.22 A.P. Baskakov, *Int. Chem. Engin.*, **4**, 320 (1964).
- 3.23 N.I. Gelperin, V. G. Einstein, A. V. Zakovski, *Khim. Prom.*, **6**, 418 (1966).
- 3.24 N.I. Gelperin and V. G. Einstein, *Fluidization* (Edited by Davidson and Harrison), Academic Press, London, 471 (1971).
- 3.25 W.N. Sullivan and R. H. Sabersky, "Heat Transfer to Flowing Granular Media," *Int. J. Heat Mass Trns.*, **18** (1), 97-107 (1975).
- 3.26 R. Nietert, "Heat Transfer Characterization of Flowing and Stationary Particle Bed Type Fusion Reactor Blankets," Ph.D. Thesis, Nuclear Engineering Dept. University of Wisconsin, Madison (1982).
- 3.27 R.G. Deissler and J.S. Boegli, "An Investigation of Effective Thermal Conductivities of Powders in Various Gases," *Trans. ASME*, **80** (7), 1417-1425 (1958).
- 3.28 R.D. McCarty, "Thermophysical Properties of Helium-4 from 2-1500 K with Pressure to 1000 Atmospheres," National Bureau of Standards, Boulder, CO (1972).
- 3.29 W.V. Green, D.L. Smith, and B.T. Kelly, "Summary of the RIGI-KALTBAD Workshop on Graphite," *J. of Nucl. Mater.*, **122&123**, 14-16 (1984).
- 3.30 R.D. O'Dell et al., "User's Manual for ONEDANT: A Code Package for One-Dimensional, Diffusion-Accelerated, Neutral Particle Transport," Los Alamos National Laboratory Report, LA-9184-M (1982).
- 3.31 B. Badger et al., "LIBRA - A Light Ion Beam Fusion Conceptual Reactor Design," University of Wisconsin Fusion Technology Institute Report UWFD-800 (1989).
- 3.32 M. Birch and J.E. Brocklehurst, "A Review of the Behavior of Graphite Under the Conditions Appropriate for Protection of the First Wall of a Fusion Reactor," Springfield Nuclear Power Development Lab., ND-R-1434(S) (Dec. 1987).
- 3.33 M.C. Billone, C.C. Lin, H. Attaya, and Y. Gohar, "Tritium Retention and Release Analysis for US-ITER Blanket," *Fusion Technol.*, **19**, 976 (1991).
- 3.34 K.E. Plute, E.M. Larsen, and L.J. Wittenberg, "Tritium Recovery from Liquid Lithium-Lead by Vacuum Degassing," *Nuclear Tech./Fusion*, **4**, 407 (1983).

- 3.35 C.E. Johnson and A.K. Fischer, "Blanket Materials for Fusion Reactors: Comparisons of Thermochemical Performance," *J. Nuclear Materials*, **130**, 445 (1985).
- 3.36 M.C. Billone and C.C. Lin, "Input for Tritium Retention/Release Analysis and Steady-State Results," presented at the ITER Nuclear Group Mtg. (May 9, 1990).
- 3.37 S. Tanaka, A. Kawamoto, D. Yamaki, K. Yamaguchi, and M. Yamawaki, "In situ Tritium Release Experiments from Solid Breeding Materials (TTEx) - Surface Reactors of Li<sub>2</sub>O and LiAlO<sub>2</sub> for Sweep Gases of He + H<sub>2</sub> and He + H<sub>2</sub>O," *J. Nuclear Materials*, **179-181**, 867 (1991).
- 3.38 Y. Hirooka and H. Imai, "Reaction of Neutron Irradiated Pyrolytic Graphite with Water Vapor," *JAERI-Memo*, 57-218 (1982).
- 3.39 A. Busigin, S.K. Sood, and K.M. Kalyanan, "A New High Temperature Isotopic Exchange Fuel Processing Loop Design for ITER," *Fusion Technol.*, **20**, 179 (1991).
- 3.40 J.T. Bell, J. D. Redman, and H.F. Bittner, "Tritium Permeability of Structural Materials and Surface Effects on Permeation Rates," Proc. ANS Topical Meeting on Tritium Technology, Dayton, OH, April 29-May 1, 1980, pp. 48-53 (CONF-800427).
- 3.41 J.L. Anderson et al., "Experience of TSTA Milestone Runs with 100 Gram-level of Tritium," *Fusion Technol.*, **14**, 438 (1988).
- 3.42 R.A. Causey, M. I. Baskes, and K.L. Wilson, "The Retention of Deuterium and Tritium in POCO AXF-5Q Graphite," *J. Vac. sci. tech.*, **A4**, 1189 (1986).
- 3.43 K.B. Woodall, S.K. Sood, and A. Busigin, "Conceptual Design of a Laboratory Scale Impurity Detritiation and Hydrogen Isotope Separation System," *Fusion Technol.*, (1991), in press.
- 3.44 C.J. Sienkiewicz, "Tritium Surface Contamination," *Fusion Technol.*, **8**, 2444 (1985).
- 3.45 R.L. Bieri and M. W. Guinan, "Grazing Incidence Metal Mirrors as the Final Elements in a Laser Driver for Inertial Confinement Fusion." *Fusion Technol.*, **19** (May 1991).
- 3.46 R.C. Davidson et al. "Inertial Confinement Fusion Reactor Design Studies Recommended Guidelines" prepared for Department of Energy Office of Fusion Energy (Sept. 1990).
- 3.47 R.R. Berggren, R.L. Gibson, R.H. Lehmborg, and C.W. vonRosenberg, Jr., "Large KrF Lasers as High-Brightness, High-Energy Sources," also D.B. Harris, et al. "Strengths and Weaknesses of KrF Lasers for ICF Applications Learned from the AURORA Laser," IAEA Technical Committee Meeting on Drivers for Inertial Confinement Fusion, Osaka, Japan, (April 15-19, 1991).
- 3.48 M. McGeoch "A High Current Density Non-Closing Plasma Cathode," *J. Appl. Phys.*, **71** (3), 1163 (1 Feb. 1992); also U.S. Patent No. 5,003,226.
- 3.49 J.H. Pendergrass, *Fusion Technol.*, **11**, 732 (1987).
- 3.50 J.A. Sullivan, "A Simplified Model for Designing Large KrF Amplifiers," Los Alamos, NM 87545

- 3.51 This value is consistent with presentation of Y. Owandano "High Power KrF Laser System, ASHURA," Paper WA-1, KrF Laser Technology Workshop, Santa Fe, April 19-21, 1989; also R.H. Lehmberg "Optical Beam Smoothing in the NIKE Laser," presentation to Fusion Policy Advisory Committee, Berkeley, May 10, 1990 -  $Q > 3$  mrad is suggested; the LMF design assumed 5 mrad.
- 3.52 D.B. Harris, J.A. Sullivan, J.H. Pendergrass, N.A. Kurnit, E.A. Rose, and J. McLeod "KrF Laser-Driven Laboratory Microfusion Facility," Los Alamos National Laboratory LA-UR-91-2915 (Dec. 17, 1991).
- 3.53 J.A. Sullivan and C.W. von Rosenberg, Jr. "High energy krypton fluoride lasers for laser-induced fusion," *Lasers and Particle Beams*, **4**, 91 (1986).
- 3.54 J.H. Parks "Angular multiplex laser fusion drivers," Proceedings of SPIE **270**, 81 (1981); also J.H. Parks "Conceptual Design of an Angularly-Multiplexed Rare Gas Halide Laser Fusion Driver," Avco final report for DoE contract DE-AC08-79DP40113 (Nov. 1980).
- 3.55 "Conceptual Design of a 1.5MJ, 2Hz KrF Fusion Laser System," Lawrence Livermore Lab Report, UCRL-53077 (1980).
- 3.56 R. Limpaecher, R. Litte, and S. Ghoshroy, "High Voltage Cable PFL Test Results," 17th Power Modulator Symposium, Seattle, WA (June 23-25, 1986).
- 3.57 J.C. Martin, AWRE report SSWA/JCM/704/49 (1970).
- 3.58 J.H. Parks "Conceptual Design of an Angularly-Multiplexed Rare Gas Halide Laser Fusion Driver," Avco final report for DoE contract DE-AC08-79DP40113 (Nov. 1980).
- 3.59 R. Limpaecher and S. Ghoshroy, unpublished data (1987).
- 3.60 M.A. Gundersen and G. Schaefer, "Physics and Applications of Pseudosparks," Plenum Press, New York (1990).
- 3.61 M.W. McGeoch, A.J. DeFuria and C.T. Pike "Pulsed Electric Discharge Laser Technology - Electron Beam Window Foil Material," report for Contract DAAH01-82-D-A013, (1984).
- 3.62 C.W. von Rosenberg, Jr., "Repetatively Pulsed KrF Amplifiers for Laser Fusion," Final Report of Task 3 of Contract No. 9-XT9-E9580-1 (Nov. 1990).
- 3.63 D.B. Harris, J.A. Sullivan, J.H. Pendergrass, N.A. Kurnit, E.A. Rose, and J. McLeod, "KrF Laser-Driven Laboratory Microfusion Facility," Los Alamos National Laboratory LA-UR-91-2915 (Dec. 17, 1991).
- 3.64 T. Izawa et al., Syowa Optical Co., Ltd., Japan, "Laser Damage Thresholds of Optical Coatings for High Power Lasers," presented at IAEA Technical Committee Meeting on Drivers for Inertial Confinement Fusion, Osaka, April, 1991.; see also Los Alamos Report LA-UR-91-2915, KrF Laser Driven Laboratory MicroFusion Facility - Conceptual Design Report, David B. Harris, et al. (Dec., 1991).
- 3.65 L.A. Rosocha, J. McLeod and J.A. Hanlon, "Beam Propagation Considerations in the Aurora Laser System," *Fusion Technol.* **11**, 624 (1987).
- 3.66 A.V. Deniz, M.S. Pronko, S.P. Obenschain, R.H. Lehmberg "Production of Flat KrF Focal Profiles for Laser Fusion Experiments," CLEO'91 (1991).